Available online at www.sciencedirect.com
ScienceDirect
International Journal of Mass Spectrometry 265 (2007) 308–325
International Journal of Mass Spectrometry
www.elsevier.com/locate/ijms

Binding energies for the inner hydration shells of Ca^{2+}: An experimental and theoretical investigation of $Ca^{2+}(H_2O)_x$ complexes ($x = 5$–9)

Damon R. Carl, Robert M. Moision, P.B. Armentrout *

Department of Chemistry, University of Utah, 315 S. 1400 E., Room 2020, Salt Lake City, UT 84112, United States

Received 20 November 2006; received in revised form 8 March 2007; accepted 8 March 2007
Available online 12 March 2007

In honor of Jean Futrell and in thanks for his many notable contributions to ion dynamics, ion chemistry, and collision-induced dissociation.

Abstract

The sequential bond energies of $Ca^{2+}(H_2O)_x$ complexes, where $x = 5$–9, are determined by collision-induced dissociation (CID) using a guided ion beam tandem mass spectrometer with a recently developed electrospray ionization source. To our knowledge, this represents the first quantitative threshold CID study of multiply charged ions. The kinetic energy dependent cross sections are determined over a wide energy range to monitor all possible dissociation products and are modeled to obtain 0 and 298 K binding energies for loss of a single water molecule. These binding energies decrease monotonically for the $Ca^{2+}(H_2O)_5$ complex to $Ca^{2+}(H_2O)_7$ and plateau for $Ca^{2+}(H_2O)_7$, $Ca^{2+}(H_2O)_8$, and $Ca^{2+}(H_2O)_9$. This suggests that six water molecules bind directly to the calcium ion and that three outer shell water molecules bind to inner shell water molecules through similar binding motifs. Our experimental results agree well with previous literature results obtained by equilibrium and BIRD studies. We also present an in-depth theoretical study of the structures and energetics of the $Ca^{2+}(H_2O)_x$ systems, employing several levels of theory. The present theoretical results focus on the larger hydrates ($x = 8$ and 9) where multiple low lying conformations are possible and there is little previous theory.

Keywords: Calcium ion; Collision-induced dissociation; Guided ion beam mass spectrometry; Hydration enthalpy; Multiply charged ion

1. Introduction

Calcium ions play a significant role in a number of physiological processes. As an example, the concentration of free calcium ions within the cytosol of a muscle cell must be maintained between 10^{-6} and 10^{-7} M to induce muscle contraction [1]. Intracellular calcium concentrations are governed by ions coming in and out of the cell via ATP driven calcium ion channels within the cellular membrane, in and out of internal storage facilities (sarcoplasmic reticulum), or regulated by calmodulin, a calcium-regulating protein. For these calcium ions to bind to calmodulin, they must go from a completely hydrated state to one that is semi-hydrated, at which point ligand exchange occurs between the remaining water molecules and oxygen containing side chains of the protein molecule. Studying the complete dehydration of the calcium ion is a critical building block for a detailed understanding of such ligand exchange reactions.

The stepwise dehydration of a number of singly charged metal ion (M^+) hydrates has been previously investigated experimentally using equilibrium [2–4] and guided ion beam techniques [5–8]. These metal ion hydrates are formed by three-body associative reactions after generating M^+ in the gas phase in the presence of water vapor. Using this type of approach to study doubly charged ion hydrates is troublesome because the second ionization energy of most metals exceeds the first ionization energy of water (12.6 eV) [9]. Thus, association reactions may not lead to $M^{2+}(H_2O)_x$, but rather to two singly charged species, $MOH^+(H_2O)_x$ and $H_3O^+(H_2O)_x$ [10,11]. As a result, alternative sources for efficiently generating such $M^{n+}(H_2O)_x$ species are desirable. One attractive possibility is to use electrospray ionization (ESI) where ions that exist in solution can be transferred directly into the gas phase [12,13].

The present work presents results obtained using a newly developed ESI source that enables us to generate metal ion hydrates. In the present work, we investigate the energetics for single water molecule loss of the $Ca^{2+}(H_2O)_x$ system, where $x = 5$–9, using threshold collision-induced dissociation (TCID). TCID studies are well established means of acquiring

* Corresponding author. Tel.: +1 801 581 7885; fax: +1 801 581 8433.
E-mail address: armentrout@chem.utah.edu (P.B. Armentrout).

1387-3806/$ – see front matter © 2007 Elsevier B.V. All rights reserved.
doi:10.1016/j.ijms.2007.03.008

accurate bond energies of ligated metal systems, but quantitative TCID studies have not heretofore been performed on multiply charged metal–ligand systems. Therefore, the hydration of doubly charged calcium ions is also of interest because we can compare the experimental binding energies of the $Ca^{2+}(H_2O)_x$ complexes derived here with those from the literature to test the accuracy of our experimental approach. Ca^{2+} hydration has been studied previously by a number of experimental methods. Kebarle and coworkers have investigated the stepwise dehydration of $Ca^{2+}(H_2O)_x$ where $x = 6$–14, using high pressure mass spectrometry (HPMS) equilibrium experiments [10,14]. Williams and coworkers have also studied the $Ca^{2+}(H_2O)_x$ systems ($x = 5$–10) using kinetic experiments of blackbody infrared radiative dissociation (BIRD) [15,16]. In addition to these quantitative studies, Shvartsburg and Siu have qualitatively studied the critical size for the $Ca^{2+}(H_2O)_x$ systems, i.e., the size at which a proton transfer/charge separation process becomes competitive with single ligand loss [11].

Because experimentalists have yet to fully understand the binding of water molecules making up the inner hydration shell of calcium, much theoretical work has been done to fill this void. Theoretical calculations employing a diverse group of basis sets and levels of theory have been used to study these tightly bound water molecules, whereas larger $Ca^{2+}(H_2O)_x$ complexes that involve the second solvent shell have generally not been included [17–20]. As our data analysis requires reliable molecular parameters, the present study provides an in-depth theoretical look at the structures and energetics of the $Ca^{2+}(H_2O)_x$ systems ($x = 1$–9), including those where second shell water molecules hydrogen bond to the inner hydration shell. By comparing our experimental results with these theoretical calculations, we provide a more extensive understanding of the geometric structures of the inner and outer hydration shells.

2. Experimental and computational methods

2.1. General experimental procedures

Cross sections for the CID of the $Ca^{2+}(H_2O)_x$ complexes are measured using a guided ion beam tandem mass spectrometer (GIBMS) that has been previously described in detail [21,22]. The $Ca^{2+}(H_2O)_x$ complexes are produced as described below. Briefly, ions are extracted from the source and mass selected using a magnetic momentum analyzer. These ions are then decelerated to well-defined kinetic energies and focused into a radio frequency (rf) octopole ion guide, trapping the ions radially. The octopole minimizes reactant and product ion loss resulting from scattering. The octopole is surrounded by a static gas cell containing a collision gas, Xenon, at pressures between 0.03 and 0.13 mTorr. Xenon is used for reasons outlined elsewhere [6,23]. After collision, unreacted parent and product ions drift to the end of the octopole where they are mass selected using a quadrupole mass filter and detected using a scintillation ion detector capable of single ion counting.

The ion intensities are converted to absolute cross sections as described previously [21]. The uncertainty in the absolute cross sections is estimated to be ±20%. In the octopole reaction region, ions are accelerated by V_{Lab}, nominally the voltage difference between the dc bias on the octopole ion beam guide and the ion source. Because the ions are doubly charged, their kinetic energy in the laboratory frame is twice this voltage, $E_{Lab} = 2 \times V_{Lab}$. These laboratory frame energies (E_{Lab}) are converted to center-of-mass (CM) collision energies by $E_{CM} = E_{Lab} \times m/(m+M)$, where m and M represent the mass of the neutral collision gas and ionic species, respectively. The absolute zero of energy for the ion beam is determined using a retarding potential technique [21]. The derivative is then fit to a Gaussian distribution with FWHM ranging from 0.1 to 0.2 eV. The uncertainty in the absolute energy scale is 0.05 eV (lab). All energies in this paper are in the CM frame, unless noted otherwise.

2.2. Ion source

Ions are generated using our recently developed, electrospray ionization (ESI) source as described in detail elsewhere [24]. The new source comprises an electrospray needle, desolvating capillary, ion funnel, and hexapole ion guide/collision cell. $Ca^{2+}(H_2O)_x$ complexes are generated by pumping dilute (10^{-4} M) $CaCl_2$ solutions through a 0.0025 in. i.d. (35 gauge) steel capillary at very low flow rates, 0.01–0.10 mL/h, with a syringe pump. Voltages on the electrospray needle depend on the solvent used and location of the needle with respect to the inlet plate, but typical operating conditions for water are between 1.9 and 2.1 kV. The desolvating capillary (0.020, 0.030, or 0.040 in. i.d.) following the spray needle sits at a much lower voltage, less than 50 V, facilitating ion introduction into the instrument. The temperature of the desolvating capillary can be varied from room temperature to over 200 °C. Higher temperatures are needed to remove additional solvent molecules from the initial ESI spray, thus producing smaller $Ca^{2+}(H_2O)_x$ complexes. The desolvating capillary is 4 in. long and its exit is flush with the first plate of the ion funnel.

The rf/dc ion funnel is an rf ion guide used to transfer ions from a high pressure region to one of lower pressures while concentrating them to a smaller radius. Prior evidence has shown that ion funnels increase signal intensity by reducing scattering of the ions compared with static voltage lenses [25,26]. The ion funnel used here is similar to the design by Smith and coworkers with 0.020 in. brass plates separated by 0.020 in. Teflon spacers [27]. The first region (drift region) of the funnel has 24–28 plates with centered holes of 1.000 in. diameter. After this region, the final 60 plates have holes decreasing in diameter by 0.014–0.015 in. per plate until the last plate has a diameter of 0.096 in. A dc-only injection lens with a diameter of 0.125 in. follows the last ion funnel plate. A linear voltage drop over the ion funnel plates is adjusted by controlling the voltage of the first and last plates of the funnel with a resistor chain connecting all intervening plates. The entrance plate voltage is typically below 15 V with the exit plate above 3 V. This voltage drop should be small enough that there is no additional heating of the ions [24]. The dc-only injection lens has a voltage between the final ion funnel plate and the hexapole dc voltage, which is typically grounded at 0 V, but can be floated. Alternate funnel plates have

alternate rf phases to radially focus the ions in the funnel using peak-to-peak voltages of 10–30 V and frequencies between 1.0 and 2.0 MHz. Both of these parameters are adjusted to maximize the ion signal of the $Ca^{2+}(H_2O)_x$ complex under study.

The final portion of the new ion source is the rf hexapole ion guide/collision cell. Multipole ion guides have been used extensively in ion-molecule experiments for effectively transporting ions from high to low pressure regions [28]. The rf hexapole, in conjunction with the ion funnel, has been shown to produce thermalized ions by comparing to results for previous CID experiments using a flow tube/dc discharge ionization source [24]. Thermal ions are assumed to be in their ground vibrational and rotational states and can be described by a Maxwell–Boltzmann distribution at room temperature. Optimum peak-to-peak rf voltages on the hexapole for the $Ca^{2+}(H_2O)_x$ complexes vary depending on the size of the ion complex. We have limited this voltage to 400 V with operating frequencies between 5 and 7 kHz.

2.3. Thermochemical analysis

The kinetic energy dependent cross sections for single water molecule loss from a parent $Ca^{2+}(H_2O)_x$ complex are modeled using the empirical threshold model shown in Eq. (1):

$$\sigma(E) = \frac{\sigma_0 \sum g_i (E + E_i - E_0)^n}{E} \quad (1)$$

where σ_0 is an energy independent scaling factor, E the relative translational energy of the ion, E_0 the reaction threshold at 0 K, and n is an adjustable fitting parameter that describes the efficiency of the energy transfer upon collision [22]. The summation is over the ro-vibrational states of the reactants having excitation energies, E_i, and populations, g_i, where $\sum g_i = 1$. Vibrational frequencies and rotational constants are taken from the ab initio calculations discussed below. The Beyer–Swinehart algorithm is used to evaluate the internal energy distribution for the reactants [29–32]. The relative populations, g_i, are computed for a Maxwell–Boltzmann distribution at 300 K.

To produce accurate thermochemical data from the modeling of the CID process, we must consider a number of effects such as those arising from multiple collisions, lifetime effects, and energy distributions. To insure rigorous single collision conditions, cross sections are obtained at multiple pressures, typically about 0.030, 0.075, and 0.125 mTorr in these studies, and extrapolated to zero pressure cross sections [33,34]. As the $Ca^{2+}(H_2O)_x$ ions become more complex, ions with excess energy of the threshold energy may not have time to dissociate on the timescale of the experiment, about 5×10^{-4} s [22]. This leads to a kinetic shift in the energy threshold obtained from our modeling. To account for this effect, we incorporate Rice–Ramsperger–Kassel–Marcus (RRKM) statistical theory [32] for unimolecular dissociation into Eq. (1), as discussed in detail previously [35–37] and shown in Eq. (2).

$$\sigma(E) = \left(\frac{n\sigma_0}{E}\right) \sum_i g_i \int_{E_0 - E_i}^{E} [1 - e^{-k(\varepsilon + E_i)\tau}](E - \varepsilon)^{n-1} \, d\varepsilon \quad (2)$$

Here, ε represents the energy deposited into the ion upon collision with Xenon, τ the average timescale of the experiment (ion time-of-flight from the collision cell to the quadrupole mass spectrometer), and $k(\varepsilon + E_i) = k(E^*)$ is the RRKM unimolecular dissociation rate constant shown in Eq. (3),

$$k(E^*) = \frac{s N_{vr}^{\dagger}(E^* - E_0)}{h \rho_{vr}(E^*)} \quad (3)$$

where s is the reaction degeneracy calculated from the ratio of rotational symmetry numbers of the reactants with respect to the products, $N_{vr}^{\dagger}(E^* - E_0)$ is the sum of the ro-vibrational states of the transition state at an energy $E^* - E_0$ above the threshold, E_0, and $\rho_{vr}(E^*)$ is the density of ro-vibrational states for the energized molecule at the energy available, E^*. When the rate constant is much faster than the average experimental timescale, Eq. (2) reduces to Eq. (1). The integration in Eq. (2) is over the excitation energy distribution, which is a function of the impact parameter between the ion and Xenon gas. Eq. (2) has been shown to accurately describe kinetic shifts in a number of previous CID experiments [38–43].

The calculation of the RRKM unimolecular rate constant requires the ro-vibrational states of the energized molecule (EM) and transition state (TS) [32,44,45]. The molecular parameters for the EM are taken from ab initio calculations of the reactant ion. The TS is assumed to be loose with no reverse activation barrier, as is appropriate for the heterolytic bond cleavages studied here [46]. Thus, the phase-space limit (PSL) TS is product-like using molecular parameters taken from ab initio calculations of the products. For the $Ca^{2+}(H_2O)_x$ complexes, the transitional modes, those that become rotations of the dissociated products, are treated as rotors and calculated from the rotational constants of the separate dissociation products, $Ca^{2+}(H_2O)_{x-1}$ and H_2O. The external rotational constants and rotational energy of the TS are determined by assuming that the TS is located at the centrifugal barrier for the interaction of $Ca^{2+}(H_2O)_{x-1}$ and H_2O, and calculated using a variational approach as outlined elsewhere [37]. The data analysis program used (CRUNCH) accurately accounts for the charge on the ion in determining the location of the centrifugal barrier. The 2D external rotations are treated adiabatically, but include centrifugal effects [47]. Here, the adiabatic 2D external rotational energy of the EM is calculated using a statistical distribution with an explicit summation over the possible values of the rotational quantum number [37].

The model CID cross sections of Eqs. (1) and (2) are convoluted over the kinetic energy distributions of the $Ca^{2+}(H_2O)_x$ complex and Xenon gas, then compared with the experimental cross sections [21]. A nonlinear least squares fitting procedure is used to optimize the fitting parameters of Eq. (1) or (2), σ_0, n, and E_0. Because E_0 represents the minimum amount of energy required to go from reactants to products at 0 K, this reaction threshold represents the binding energy of the water molecule to the complex. This assumes that there are no activation barriers beyond the endothermicity of the reaction, which is ordinarily the case for heterolytic bond cleavages such as those studied here [46]. The uncertainty associated with the reaction threshold, E_0, is determined from additional modeling of the cross sections

by scaling the ab initio vibrational frequencies up and down by 10%, varying the best fit n value up and down by 0.1, and if lifetime effects are taken into account, by scaling the average experimental time available for dissociation up and down by a factor of two. The absolute uncertainty of the energy scale (0.05 eV lab) is also included.

2.4. Computational details

All theoretical calculations were done using Gaussian03 unless noted otherwise [48]. Geometry optimizations for the $Ca^{2+}(H_2O)_x$ complexes are calculated using density functional theory (DFT) with Becke's three parameter (B3) functional [49] and the correlation functionals of Lee, Yang, and Parr (LYP) [50] with a 6-311+G(d,p) basis set. Vibrational frequencies and rotational constants used in the modeling procedures are obtained at this same level of theory. Vibrational frequencies are scaled by 0.989 when used in modeling or to calculate the zero-point energy (ZPE) and thermal correction for a given complex. This scale factor is taken from Bauschlicher and Partridge for vibrational frequencies calculated using the 6-311+G(3df,2p) basis set, which includes additional polarization functions compared with the 6-311+G(d,p) basis set used here [51]. Single point energies are then calculated using B3LYP, B3P86 [52], and MP2(full) [53] levels of theory with a 6-311+G(2d,2p) basis set at the B3LYP/6-311+G(d,p) geometries. ZPE and thermal corrections were calculated for the reactants and subsequent products using the scaled frequencies as described above. Basis set superposition error (BSSE) corrections were also calculated using the full counterpoise (CP) method [54,55].

The 6-311+G(d,p) basis set used for geometry optimizations is a bit larger than the basis sets used for prior theoretical calculations in our laboratories [38,41]. Previous work in our group has suggested that the use of diffuse functions for the initial optimization is important to better handle hydrogen bonding within $K^+(L)$ complexes where L = glycine and complexes that contain functional components of glycine [42]. Because hydrogen bonding is of utmost importance to properly describe the structures of larger hydrated complexes as well as the orientation of the water molecules in $Ca^{2+}(H_2O)_x$ ($x = 5$ and 6), a larger basis set is desirable to obtain the most accurate structures and energetics for single point energy calculations. Additionally, Pavlov et al. have suggested and quantitatively shown that the use of the diffuse functions on the heavy atoms is imperative to obtain accurate single point energies for divalent hydrated systems [17].

Additional geometry optimizations for the $Ca^{2+}(H_2O)_x$ complexes, where $x = 5$–7 were calculated to determine low energy structures with varying number of water molecules bound directly to the calcium ions. As the $Ca^{2+}(H_2O)_x$ complexes become larger ($x > 7$), it becomes possible that structures may have multiple low-lying conformations within a few kJ/mol of the lowest energy structure. We have located such conformations using a simulated annealing procedure that has been described in detail previously [43]. Our findings for these alternate structures and their relative energies are presented below.

To test the accuracy of our theoretical calculations, we have followed the same protocol as for the B3LYP calculations but have used Möller Plesset second-order perturbation theory, MP2(full), for initial geometry optimizations [53]. ZPE and thermal corrections are taken from the scaled (0.989) B3LYP frequency calculations described above. BSSE corrections at the full counterpoise level were calculated using the 6-311+G(2d,2p) basis set following the same protocol as above.

In addition to the all-electron basis sets, split basis set calculations have been utilized for comparison of experimental and theoretical binding energies. Previous work in our group [38] on $K^+(NH_3)_x$ complexes has shown that the use of relativistic Hay–Wadt [56] and Stuttgart–Dresden [57] effective core potentials (ECP) for potassium underestimates the metal–ligand binding energies. Because $Ca^{2+}(H_2O)_x$ is isoelectronic with $K^+(NH_3)_x$, pseudopotential calculations were not considered here. Another approach is to treat the light atoms with a different basis set leaving the treatment of the metal ion unchanged from the all-electron calculations. We have utilized Dunning's correlation consistent basis set, aug-cc-pVTZ [58], in conjunction with the B3LYP level of theory for initial geometry optimizations and B3LYP, B3P86, and MP2(full/FC) single point energy calculations. The aug-cc-pVTZ basis set does not include parameters for Ca; therefore, a number of combinations using the aug-cc-pVTZ basis on water along with different of basis sets on Ca were employed. These include a 6-311+G(d) basis set on Ca for geometry optimizations and a 6-311+G(2d) basis set for single point energies, a combination that will further be referred to as aug-cc-pVTZ(Ca-G). We also used the cc-pVTZ, cc-pCVTZ, and cc-pwCVTZ basis sets on Ca for both geometry optimization and single point energies, and these will be referred to as aug-cc-pVTZ, aug-cc-pVTZ(Ca-C), and aug-cc-pVTZ(Ca-wC) [59]. Note that the latter two basis sets include correlation of the core electrons on calcium, an effect that has proven to be valuable in accurately describing the bonding in Li^+ complexes [60]. BSSE corrections were also calculated using the same levels of theory as those for the single point energy calculations. ZPE and thermal corrections are taken directly from scaled (0.989) B3LYP/6-311+G(d,p) frequency calculations.

3. Results

3.1. Cross sections for collision-induced dissociation

The CID cross sections for $Ca^{2+}(H_2O)_x$ ($x = 5$–9) are shown in Fig. 1. For each reactant, we investigated a broad energy range to observe all possible dissociation products. In all cases, the dominant process is the loss of a single water molecule from the parent species, reaction (4).

$$Ca^{2+}(H_2O)_x + Xe \rightarrow Ca^{2+}(H_2O)_{x-1} + H_2O + Xe \quad (4)$$

From any given cross section, one can see that after the first water molecule dissociates, additional water molecules dissociate sequentially as the translational energy increases until the bare metal ion appears. A proton transfer/charge separation process, reaction (5),

$$Ca^{2+}(H_2O)_2 + Xe \rightarrow CaOH^+ + H_3O^+ + Xe \quad (5)$$

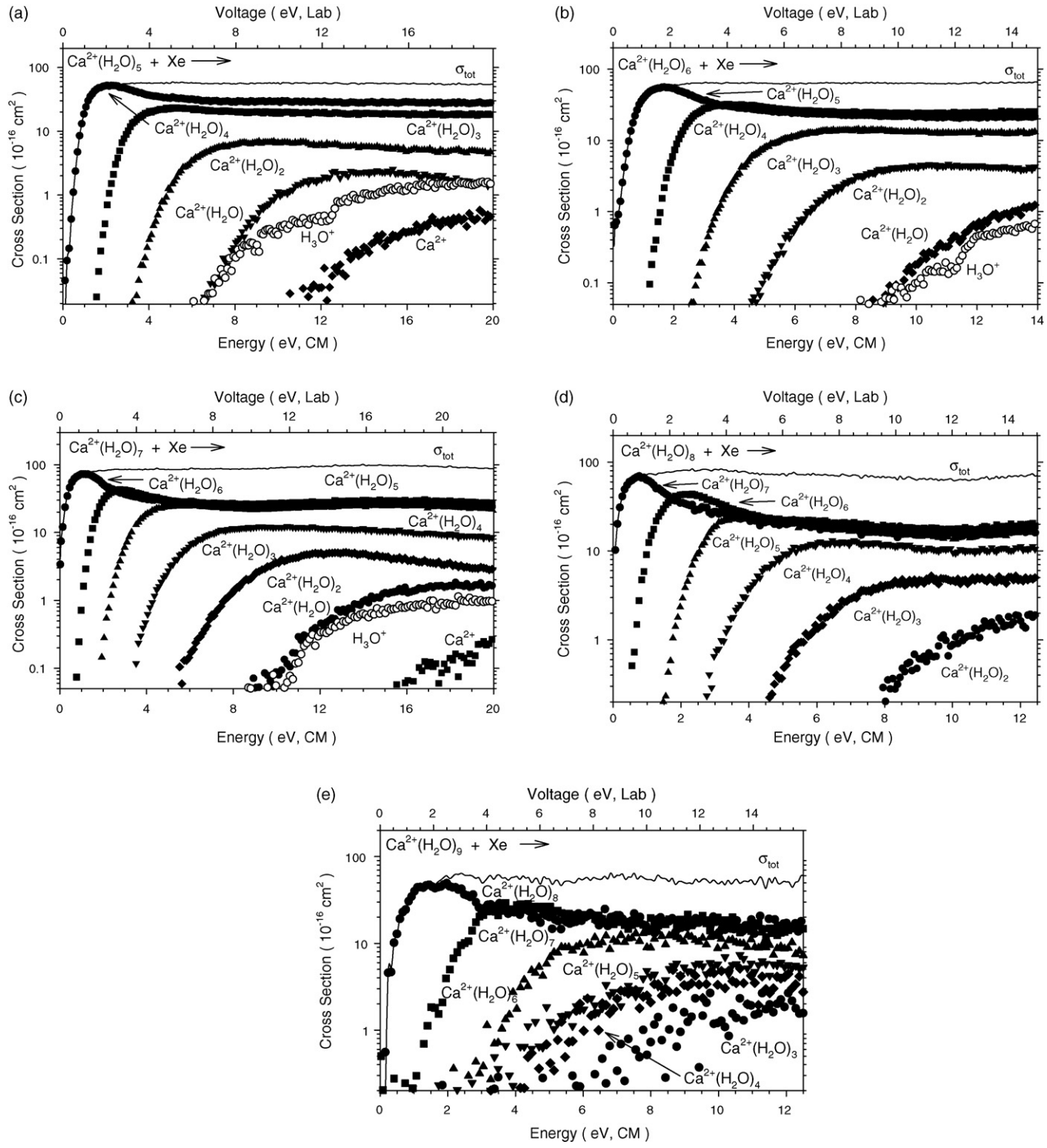

Fig. 1. Cross sections for collision-induced dissociation of $Ca^{2+}(H_2O)_x$ where $x = 5$–9 (parts a–e, respectively) with Xenon as a function of kinetic energy in the center-of-mass frame (lower x-axis) and applied voltage in the laboratory frame (upper x-axis).

is also observed within the sequential dissociation of the $Ca^{2+}(H_2O)_x$ species, and can be seen for the CID of $Ca^{2+}(H_2O)_{5–7}$ (Fig. 1a–c). Reaction (5) is observed once the $Ca^{2+}(H_2O)_2$ complex is formed. The apparent threshold for this process is close to the apparent threshold for losing an additional water molecule giving $Ca^{2+}(H_2O)$. The energy range for the CID of $Ca^{2+}(H_2O)_8$ and $Ca^{2+}(H_2O)_9$ complexes were not broad enough to see the charge separation products.

The cross sections in Fig. 1 do not show the second singly charged ion, $CaOH^+$ (m/z 57), because of mass overlap with the much more intense $Ca^{2+}(H_2O)_4$ product (m/z 56). Interestingly, no other calcium hydroxide product ions, $CaOH^+(H_2O)_y$, or proton-bound water clusters, $H^+(H_2O)_{x-y}$, were observed

for any reactant complex. As a result, the $Ca^{2+}(H_2O)_2$ complex represents a critical size for the calcium water system in which simple ligand loss becomes a competitive process with the proton transfer/charge separation process, in agreement with observations of Shvartsburg and Siu [11]. No other processes besides reaction (5) and sequential water losses were observed in these studies.

The H_3O^+ product channels in the CID spectra for $Ca^{2+}(H_2O)_5$ and $Ca^{2+}(H_2O)_6$ exhibit a noticeable break in the data, near 12.5 eV in the lab frame. This occurs because these light product ions can backscatter in the laboratory frame and either be lost or reflected by the final lens that focuses ions into the octopole ion guide. Above 12.5 eV, the backscattered ions are reflected and thus collected by the detector, enhancing the observed signal. This lens does not affect the collection of heavier product ions, which are generally forward scattered in the laboratory frame, and thus has no impact on the threshold modeling.

3.2. Pressure dependence

One interesting observation made in the present studies was the sensitivity of the cross sections to the pressure of the collision gas. In CID studies, we routinely measure the pressure dependence of our product cross sections in order to extrapolate the cross sections to single collision conditions [33,34], thereby ensuring that the collision energy is well-defined. Because the pressures used are fairly low, 0.02–0.13 mTorr here, such that single collision conditions generally prevail, these extrapolations are usually linear in pressure. In the present work, it was found that this typical procedure led to cross sections for the primary product ions (those having the lowest thresholds) of $Ca^{2+}(H_2O)_x$, $x = 6$ and 7, being negative at the lowest energies. This result indicates that secondary collisions are contributing to the dissociations observed such that a linear extrapolation over corrects for the pressure effect. (For $x = 5$, the threshold is high enough that secondary collisions are not influential, and for $x = 8$ and 9, the thresholds are sufficiently low that single collision events dominate the cross section at all energies.) This sensitivity to pressure is a direct result of the larger charge on these species, thereby increasing the collision cross section above those usually observed for singly charged ions. To properly account for this behavior, a quadratic pressure dependence can be used to extrapolate the cross sections to zero pressure conditions or the highest pressure can be removed from a linear extrapolation. Both methods gave similar extrapolated cross sections that fall to zero at the lowest energies, as shown in Fig. 2b and c.

3.3. Thermochemical results

The total reaction cross sections for water dissociation were modeled using Eqs. (1) and (2) for all $Ca^{2+}(H_2O)_x$ complexes because the overall shape of the cross sections is influenced by the cross sections for sequential dissociation of additional water molecules. It might be noted that the cross sections for $x = 7$ and 8 could not be reproduced accurately at the lowest energies when using Eq. (1), which demonstrates the need to include lifetime effects in modeling the data. The optimum modeling parameters obtained are listed in Table 1 and the models of Eq. (2) are compared to zero pressure-extrapolated cross sections in Fig. 2. From Table 1, a noticeable kinetic shift exists between the E_0 values obtained with (PSL) and without lifetime effects accounted for in the modeling. These kinetic shifts are about the same for $x = 5$ and 6, and are slightly smaller than those for $x = 7$–9, which are similar to one another.

Reaction thresholds for loss of a single water molecule from a reactant species decrease monotonically as the complex size increases from the $Ca^{2+}(H_2O)_5$ complex to the $Ca^{2+}(H_2O)_7$ complex. The $Ca^{2+}(H_2O)_7$, $Ca^{2+}(H_2O)_8$, and $Ca^{2+}(H_2O)_9$ complexes have nearly identical bond energies. These observations suggest two conclusions. First, it seems likely that six water molecules bind directly to the calcium ion and thus reside in the inner solvent shell. Second, because the larger calcium ion hydrates have similar bond energies, their hydrogen bonding interactions to the inner shell water molecules are likely to be similar.

As mentioned above, the transition state for water loss is considered to be loose. A useful measure of the looseness of these transition states is the entropies of activation, $\Delta S^{\dagger}$, which are also shown in Table 1 and derived from analyses of the data at a temperature of 1000 K. In all cases, these values are positive and relatively large, consistent with a loose transition state. These values increase from the $Ca^{2+}(H_2O)_5$ to the $Ca^{2+}(H_2O)_6$ complex, decrease for the $Ca^{2+}(H_2O)_7$, and then increase again for the larger complexes. This behavior also points to a change in the $Ca^{2+}(H_2O)_7$ structure upon addition of the seventh water molecule, consistent with the hypothesis of six inner shell water molecules.

Table 1
Parameters from Eq. (2) used to model the data for collision-induced dissociation of $Ca^{2+}(H_2O)_x$ ($x = 5$–9)

Complex	σ_0[a]	n[a]	E_0 (eV)[b]	E_0 (PSL) (eV)[a]	$\Delta S^{\dagger}_{1000}$ (J/(mol K))
$Ca^{2+}(H_2O)_5$	95 (3)	0.8 (0.2)	1.30 (0.07)	1.17 (0.06)	50 (5)
$Ca^{2+}(H_2O)_6$	102 (2)	1.1 (0.2)	1.02 (0.06)	0.92 (0.05)	71 (5)
$Ca^{2+}(H_2O)_7$	123 (6)	1.0 (0.1)	0.89 (0.05)	0.62 (0.06)	30 (5)
$Ca^{2+}(H_2O)_8$	85 (2)	0.9 (0.1)	0.85 (0.06)	0.61 (0.03)	72 (5)
$Ca^{2+}(H_2O)_9$	57 (2)	1.8 (0.1)	0.94 (0.04)	0.60 (0.03)	75 (5)

Uncertainties are in parentheses.
[a] Parameters from modeling with Eq. (2), where lifetime effects are taken into account.
[b] Thresholds from modeling with Eq. (2) when no lifetime affects are included.

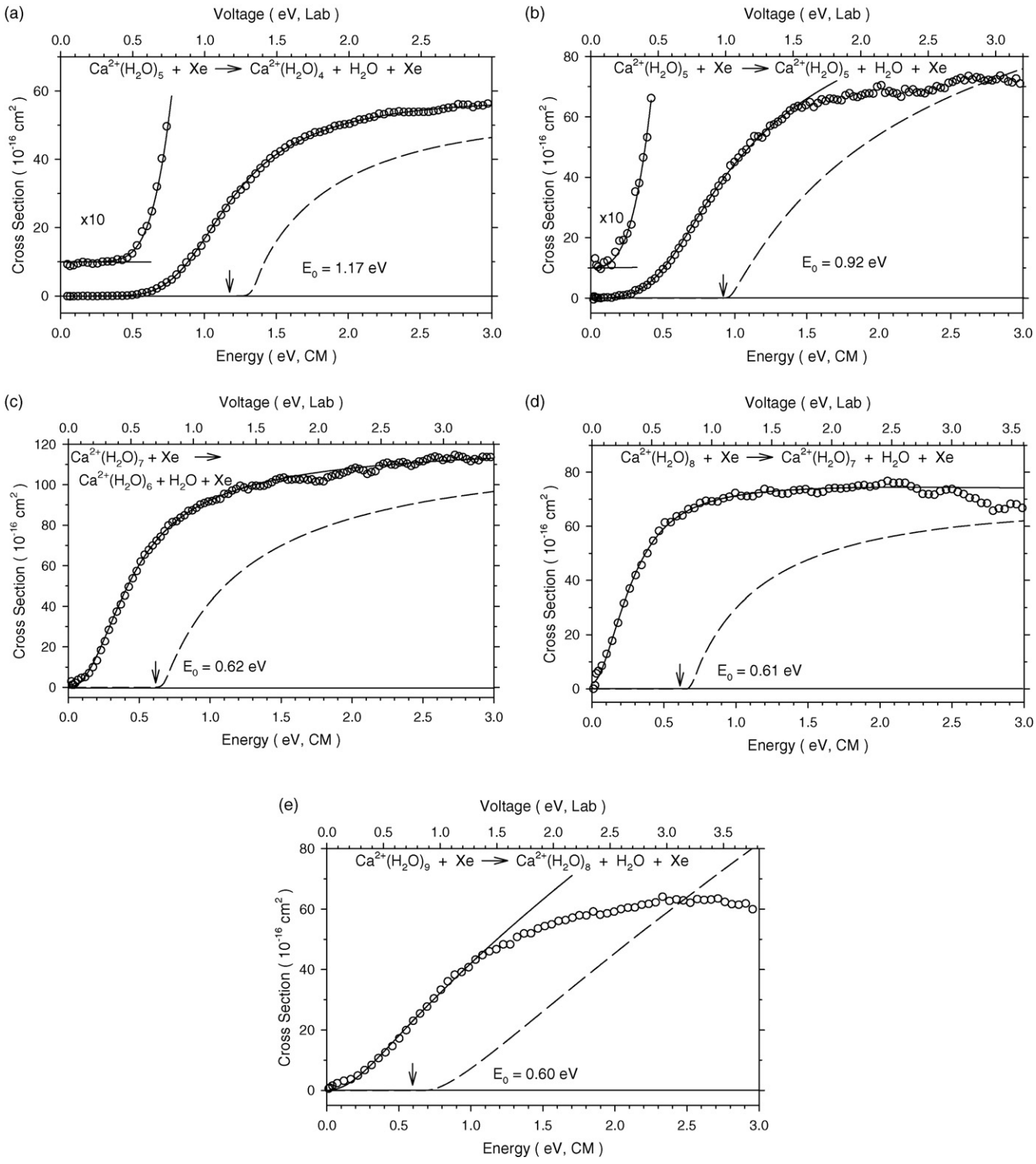

Fig. 2. Zero pressure extrapolated cross sections for collision-induced dissociation of $Ca^{2+}(H_2O)_x$ where $x = 5$–9 (parts a–e, respectively) with Xenon in the threshold region as a function of kinetic energy in the center-of-mass frame (lower x-axis) and the laboratory frame (upper x-axis). The solid lines show the best fit to the data using the model of Eq. (2) convoluted over the neutral and ion kinetic and internal energy distributions. The dashed lines show the model cross sections in the absence of experimental kinetic energy broadening for reactions with an internal energy of 0 K. The arrow indicates the threshold energy, E_0.

3.4. Theoretical geometries: overview of ground states ($x = 1$–6)

The geometry optimizations and frequency calculations for each system studied here are calculated using a B3LYP/6-311+G(d,p) level of theory. The computed molecular parameters for these complexes were used in the data analysis described above. Structures for $x = 1$–6 were first optimized without any constraints, but all converged to symmetric structures. For the smaller complexes ($x \leq 6$), we find that six water molecules are

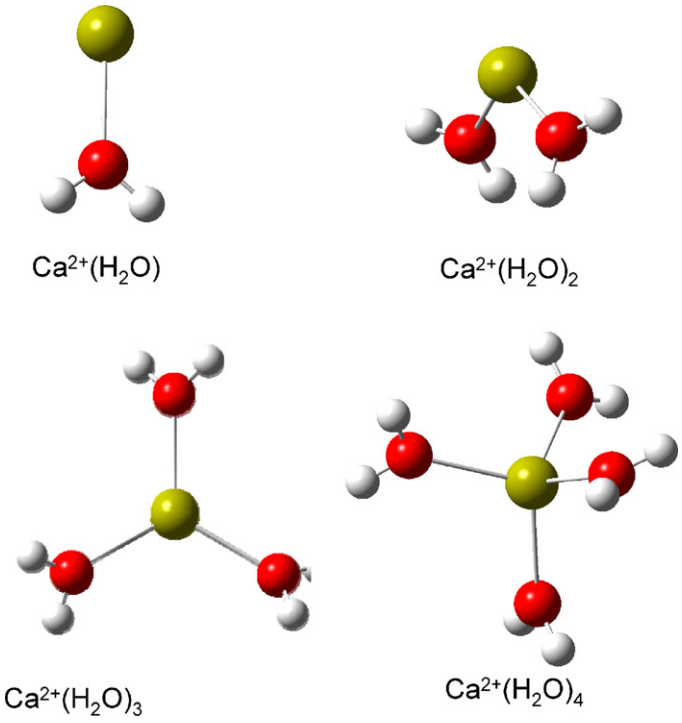

Fig. 3. Ground-state geometries of $Ca^{2+}(H_2O)_x$ where $x = 1$–4. All structures were optimized at the B3LYP/6-311+G(d,p) level of theory.

bound directly to calcium, i.e., reside in the inner solvent shell, which is in agreement with previous theoretical studies [17–20]. In all cases, these water molecules have their dipole moments directed toward the calcium cation.

Ground state structures for $Ca^{2+}(H_2O)_x$ ($x = 1$–4) are shown in Fig. 3. The single water complex has C_{2v} symmetry, as expected. Because Ca^{2+} has no valence electrons, one might expect a O–Ca–O linear configuration for the $Ca^{2+}(H_2O)_2$ complex, however, the B3LYP/6-311+G(d,p) geometry optimization predicts a bent geometry with a O–Ca–O angle of 124.7°. The orientation of the hydrogen atoms gives this structure C_2 symmetry. Such a bent structure has been calculated previously and is also found for $Sr^{2+}(H_2O)_2$, whereas $Mg^{2+}(H_2O)_2$ has a linear configuration [61]. This behavior is attributed to the core polarization of these alkaline earth metal ions, which can compensate for the increased ligand repulsion in the bent structure [61]. The MP2(full)/6-311+G(d,p) geometry optimization also converged to a bent structure with a O–Ca–O angle of 125.8° but now the hydrogen orientation gives the complex C_s symmetry (i.e., one of the water molecules is in the same plane as O–Ca–O and the other is perpendicular to this plane). This small structural disparity has little effect on the hydration enthalpies for water loss from $Ca^{2+}(H_2O)_2$ or $Ca^{2+}(H_2O)_3$. The difference between the hydration enthalpies for B3LYP/6-311+G(d,p) and MP2(full)/6-311+G(d,p) geometry optimizations is less than 1 kJ/mol.

The $Ca^{2+}(H_2O)_3$ complex has all heavy atoms in the same plane with O–Ca–O angles of 120°. The hydrogen atoms lie above and below this plane such that the complex exhibits D_3 symmetry. The HOCaO dihedral angle, where the second oxygen atom refers to the oxygen atom that the hydrogen atom points toward, is 37.0°. The $Ca^{2+}(H_2O)_4$ complex is pseudo-tetrahedral but has S_4 symmetry when the hydrogen atoms are included.

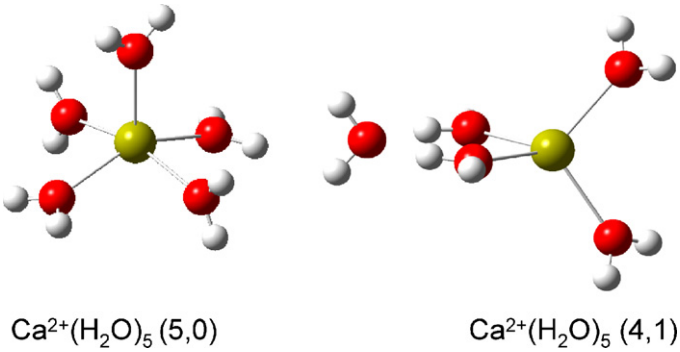

Fig. 4. Ground-state and low-lying geometries of $Ca^{2+}(H_2O)_5$. All structures were optimized at the B3LYP/6-311+G(d,p) level of theory.

Ground state structures for $Ca^{2+}(H_2O)_x$ ($x = 5$ and 6) are shown in Figs. 4 and 5, respectively. These structures are quite interesting because in both cases, hydrogen atoms from one water molecule clearly point towards the oxygen atoms on adjacent water molecules. The five water complex is pseudo square-pyramidal with the base having two sets of unique water molecules, such that the $Ca^{2+}(H_2O)_5$ complex has C_{2v} symmetry. The addition of the sixth water molecule to the five water complex puts the base of the pyramid in the same plane as the calcium ion, giving the $Ca^{2+}(H_2O)_6$ complex T_h symmetry (including hydrogen atoms).

3.5. Theoretical geometries: structural details for ground state structures (x = 1–6)

Relevant structural details of the $Ca^{2+}(H_2O)_x$ complexes, where $x = 1$–6, are listed in Table 2. Consistent with the gradually decreasing bond energies, Table 1, the Ca–O bond distances increase by about 0.03 ± 0.01 Å as each additional water molecule is added to the $Ca^{2+}(H_2O)_x$ complex. At the same time, the O–H bond distances decrease from 0.977 Å for $Ca^{2+}(H_2O)$ to 0.967 Å for $Ca^{2+}(H_2O)_6$, approaching the O–H distance of 0.962 Å for a free water molecule. The H–O–H angles increase as more water molecules surround the ion, increasing from 104.3° for $Ca^{2+}(H_2O)$ to 104.7° for $Ca^{2+}(H_2O)_4$. The $Ca^{2+}(H_2O)_5$ and $Ca^{2+}(H_2O)_6$ structures have comparable H–O–H angles (105.0–105.4°) with respect to a free water molecule (105.1°).

The structures of the $Ca^{2+}(H_2O)_5$ and $Ca^{2+}(H_2O)_6$ complexes are clearly influenced by hydrogen bonding between the inner shell water molecules. Examining the orientation of the hydrogen atoms in $Ca^{2+}(H_2O)_6$, Fig. 5, it can be seen that each hydrogen atom points towards the oxygen atom on an adjacent ligand, giving the complex T_h symmetry overall. Removal of one of the water molecules from this complex gives the pseudo-square pyramid structure of $Ca^{2+}(H_2O)_5$ (Fig. 4). Because of the hydrogen bonding, the O–Ca–O bond angles in the base of the pyramid are unequal: 161.6° for the two water molecules with hydrogens pointed at the apex water molecule such that the O–Ca–O bond angles to the apex oxygen are 99.2°, and 149.0°

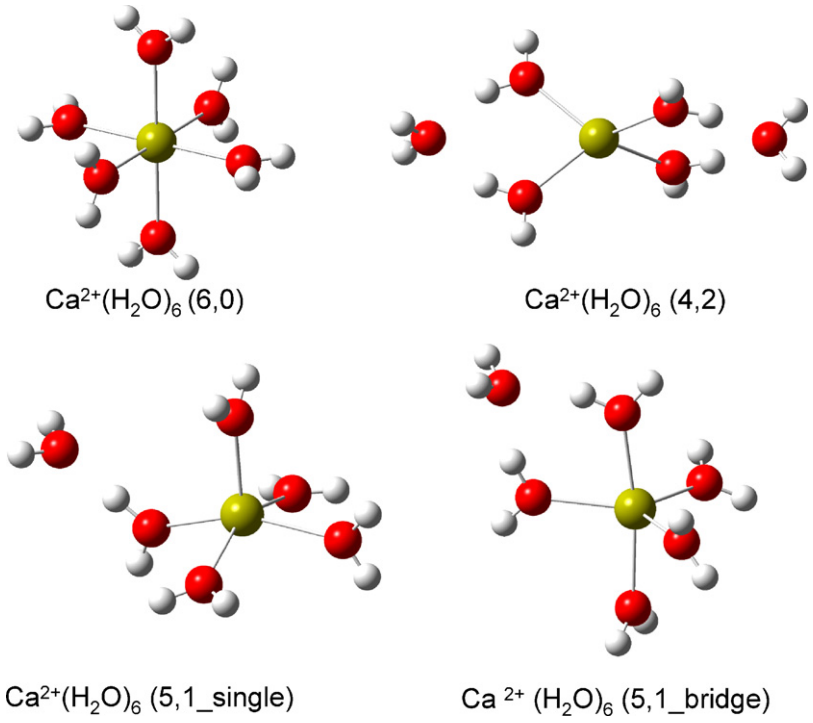

Fig. 5. Ground-state and low-lying geometries of $Ca^{2+}(H_2O)_6$. All structures were optimized at the B3LYP/6-311+G(d,p) level of theory.

for the two water molecules with hydrogens parallel with the base such that the O–Ca–O bond angles to the apex oxygen are 105.5°. The four water molecules at the base have O–Ca–O angles of 87.6° with respect to each other. The hydrogen bonding is further indicated by asymmetric Ca–O–H angles for the water molecules having a 161.6° O–Ca–O angle. Here, the hydrogen atoms pointing directly towards the apex oxygen atom have Ca–O–H angles of 126.4° whereas the hydrogen atoms not participating in the inner shell hydrogen bonding have Ca–O–H angles of 128.7°.

3.6. Theoretical geometries: alternate structures (x = 5 and 6)

Additional geometry optimizations and single point energy calculations for $Ca^{2+}(H_2O)_5$ and $Ca^{2+}(H_2O)_6$ with a different number of water molecules bound directly to the calcium ion were obtained for comparison with the ground state structures. These structures are also shown in Figs. 4 and 5. In the following discussion, the relative single point energies with respect to the ground state structures are provided in the following

Table 2
B3LYP/6-311+G(d,p) geometry optimized structures for ground state $Ca^{2+}(H_2O)_{1–6}$

Complex	Symmetry	r(CaO) (Å)	∠OCaO (°)	∠CaOH (°)	r(OH) (Å)	∠HOH (°)
H_2O	C_{2v}				0.962 (2)	105.1
$Ca^{2+}(H_2O)$	C_{2v}	2.244		127.9 (2)	0.977 (2)	104.3
$Ca^{2+}(H_2O)_2$	C_2	2.282 (2)	124.7	127.7 (2) 127.9 (2)	0.974 (4)	104.4 (2)
$Ca^{2+}(H_2O)_3$	D_3	2.313 (3)	120.0 (3)	127.7 (6)	0.972 (6)	104.5 (3)
$Ca^{2+}(H_2O)_4$	S_4	2.340 (4)	106.6 (2) 110.9 (4)	127.4 (4) 127.9 (4)	0.970 (8)	104.7 (4)
$Ca^{2+}(H_2O)_5$	C_{2v}	2.364 (1) 2.365 (2) 2.393 (2)	87.6 (4) 99.2 (2) 105.5 (2) 149.0 161.6	126.4 (2) 127.4 (6) 128.7 (2)	0.968 (4) 0.969 (6)	105.0 (2) 105.1 105.3 (2)
$Ca^{2+}(H_2O)_6$	T_h	2.405 (6)	90.0 (12) 180.0 (3)	127.3 (12)	0.967 (12)	105.4 (6)

Numbers in parentheses denote degeneracies.

order: B3LYP/6-311+G(2d,2p), B3P86/6-311+G(2d,2p), and MP2(full)/6-311+G(2d,2p), all at B3LYP/6-311+G(d,p) geometries. These results include ZPE corrections and thermal corrections to 298 K.

If four water molecules reside in the inner solvent shell with a fifth water molecule hydrogen bonded to two of these inner shell water molecules, we obtain $Ca^{2+}(H_2O)_5$ (4,1). This structure is 19.6, 16.2, and 26.7 kJ/mol higher in energy relative to the ground state $Ca^{2+}(H_2O)_5$ (5,0) complex. For the $Ca^{2+}(H_2O)_6$ complex, three additional structures were located. The (4,2) structure starts with the (4,1) structure and adds the sixth water molecule by hydrogen bonding to the two remaining inner shell water molecules. The (4,2) structure is 30.5, 23.8, and 46.6 kJ/mol higher in energy than the ground state (6,0) structure. The other two possibilities have five water molecules in the inner shell with an additional water molecule in the outer shell participating in either one (5,1_single) or two (5,1_bridge) hydrogen bonds with inner shell water molecules. These two structures are 25.5, 22.5, and 37.7 kJ/mol and 13.3, 10.0, and 23.0 kJ/mol, respectively, higher in energy relative to the highly symmetric $Ca^{2+}(H_2O)_6$ (6,0) complex. Not surprisingly, the bridging structure lies well below the structure having only a single hydrogen bond.

3.7. Theoretical geometries: ground state and low-lying structures ($x = 7$–9)

Starting structures for the larger $Ca^{2+}(H_2O)_x$ complexes were obtained using the simulated annealing program noted above. The addition of three water molecules to $Ca^{2+}(H_2O)_6$ occurs by hydrogen bonding interactions to inner shell water molecules. To better understand the lowest energy geometries of these larger structures, we start with the highly symmetrical $Ca^{2+}(H_2O)_6$ (6,0) complex. The ground state (6,1) structure of $Ca^{2+}(H_2O)_7$ is formed when two adjacent inner shell water molecules are in the same plane and form two hydrogen bonds with the outer shell water molecule (Fig. 6). This requires a rotation of 90° around any Ca–O bond, which costs roughly 10 kJ/mol at the B3LYP/6-311+G(d,p) level of theory. Two additional structures were also found for $Ca^{2+}(H_2O)_7$. The first structure has all seven water molecules binding directly to the calcium ion (7,0), as shown in Fig. 6. The (7,0) structure lies 21.9, 22.9, and 10.3 kJ/mol higher in energy than the (6,1) complex. The second structure for $Ca^{2+}(H_2O)_7$ has five water molecules binding directly to the calcium ion with each additional water molecule bridging to adjacent water molecules that make up the pyramid base for the ground state (5,0) structure (Fig. 6). The (5,2) complex is calculated to lie 3.0 kJ/mol higher for B3LYP/6-311+G(2d,2p), −0.5 kJ/mol lower for B3P86/6-311+G(2d,2p), and 13.3 kJ/mol higher for MP2(full)/6-311+G(2d,2p) single point energies with respect to the (6,1) complex.

As $Ca^{2+}(H_2O)_x$ complexes become larger ($x = 8$ and 9), an increasing number of low-lying conformations become probable. Binding of the eighth water molecule follows the same protocol as addition of the seventh water molecule: two inner shell water molecules hydrogen bonding to the oxygen atom of the outer shell water molecule. The eighth water molecule can form hydrogen bonds at a number of places on the $Ca^{2+}(H_2O)_7$ (6,1) complex. Rotation around a Ca–O bond adjacent to the first Ca–O rotation, which requires roughly 8 kJ/mol, leads to the ground state $Ca^{2+}(H_2O)_8$ (6,2) complex, Fig. 7, which nearly has C_2 symmetry.

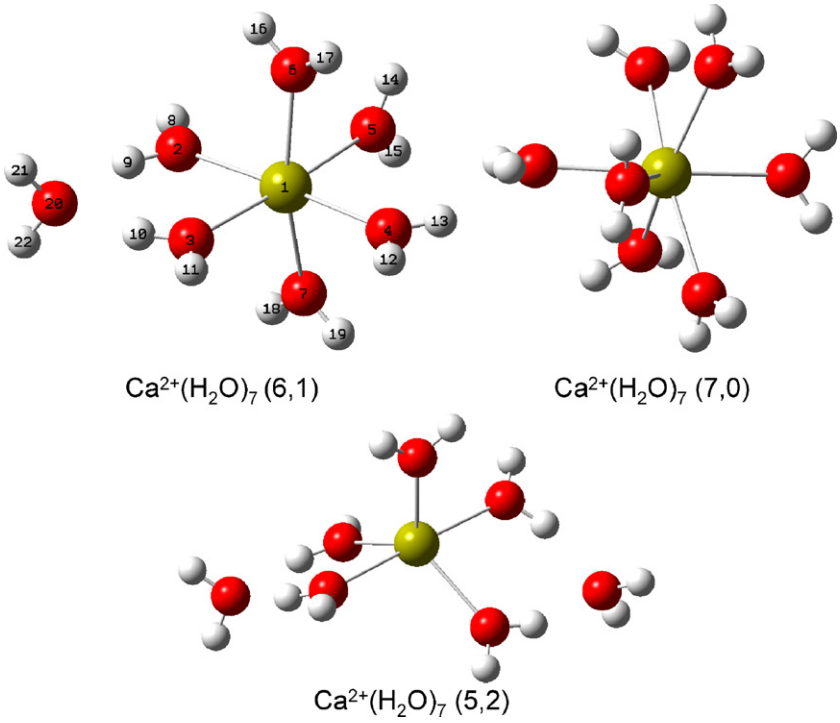

Fig. 6. Ground-state and low-lying geometries of $Ca^{2+}(H_2O)_7$. All structures were optimized at the B3LYP/6-311+G(d,p) level of theory.

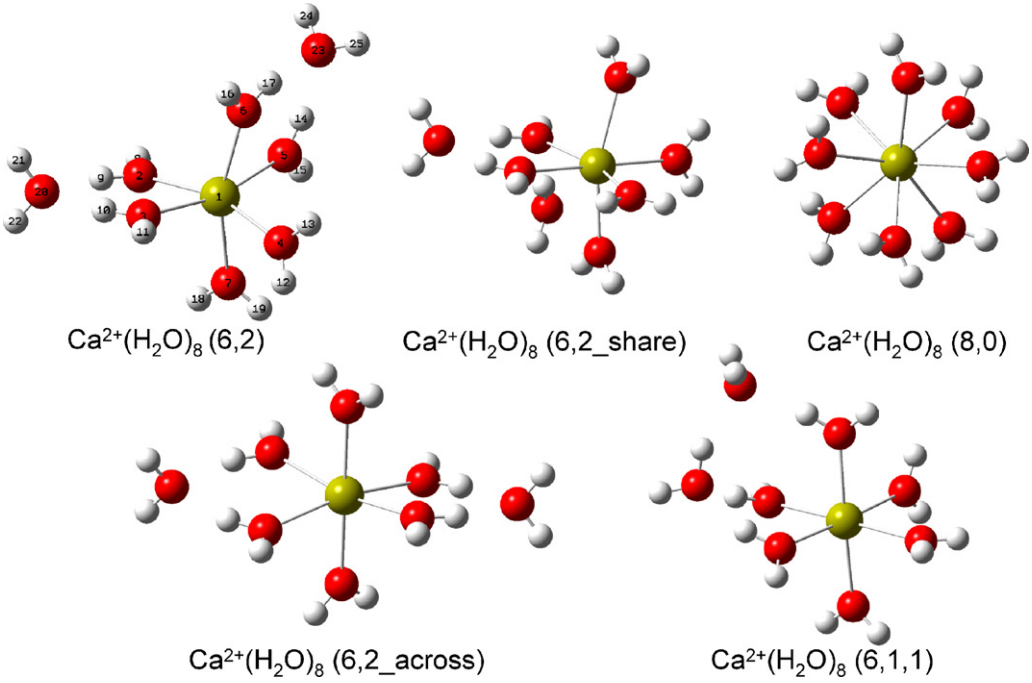

Fig. 7. Ground-state and low-lying geometries of $Ca^{2+}(H_2O)_8$. All structures were optimized at the B3LYP/6-311+G(d,p) level of theory.

The initial 90° rotation around a Ca–O bond in the $Ca^{2+}(H_2O)_6$ (6,0) complex puts three inner shell water molecules into the same plane, which allows two outer shell water molecules to hydrogen bond to these three water molecules, (6,2_share) (Fig. 7). This structure is 2.2, 2.6, and 2.6 kJ/mol higher in energy than the ground state (6,2) complex. Alternatively, rotation around the Ca–O bond directly across from the first Ca–O rotation puts the two outer shell water molecules across from one another. This (6,2_across) structure is 4.7, 4.6, and 4.7 kJ/mol higher in energy than the (6,2) complex. Another $Ca^{2+}(H_2O)_8$ structure (6,1,1), has the eighth water molecule hydrogen bonding to both an inner shell water molecule and the outer shell water molecule. The (6,1,1) structure lies 12.7, 13.1, and 11.6 kJ/mol above the (6,2) structure. Another structure has all eight water molecules binding directly to the calcium ion, (8,0). The (8,0) structure lies 41.8, 43.7, and 17.2 kJ/mol higher in energy than the ground state (6,2) complex.

The ninth water molecule hydrogen bonds to the two remaining inner shell water molecules of $Ca^{2+}(H_2O)_8$ (6,2). Rotations around both of these Ca–O bonds putting both water molecules in the same plane costs about 6 kJ/mol. This ground state $Ca^{2+}(H_2O)_9$ (6,3) complex nearly has D_3 symmetry with a C_3 axis such that each hydrogen bound second shell water molecule can rotate into one another as well as three C_2 axes around each outer shell oxygen–calcium ion bond. Three other structures were found for the $Ca^{2+}(H_2O)_9$ complex (Fig. 8). The first one builds from the $Ca^{2+}(H_2O)_8$ (6,2_share) structure. This structure has three remaining inner shell water molecules that have yet to participate in any hydrogen bonding interactions. The ninth water molecule can hydrogen bond to two of these inner shell water molecules forming the (6,3_share), which lies 4.0, 4.1, and 3.7 kJ/mol higher than the (6,3) complex. The other two $Ca^{2+}(H_2O)_9$ structures put the ninth water molecule hydrogen bonding to both an inner and outer shell water molecule of the $Ca^{2+}(H_2O)_8$ (6,2_across) and (6,2_share) structures. These structures, (6,2_across,1) and (6,2_share,1), are 15.8, 15.8, and 14.3 kJ/mol and 22.1, 21.9, and 21.9 kJ/mol higher in energy relative to the ground state (6,3) complex.

3.8. Theoretical geometries: structural details for ground state structures (x = 7–9)

Structural details for $Ca^{2+}(H_2O)_{7-9}$ are shown in Table 3. The atoms of the ground state (6,1), (6,2), and (6,3) structures are numbered in Figs. 6–8 to assist in the following discussion. The Ca–O bond distances of the inner shell water molecules (O2 and O3) that hydrogen bond to the outer shell water molecule for the ground state (6,1) complex are 2.380 Å, a decrease of 0.025 Å with respect to the Ca–O bond distances of the (6,0) complex. The average of the Ca–O bond distances for water molecules not participating in any hydrogen bonding interactions is 2.415 Å, in keeping with the increasing trend seen for $Ca^{2+}(H_2O)$ to $Ca^{2+}(H_2O)_6$. The addition of the outer shell water molecule reduces the O2–Ca–O3 bond angle to 79.7° from 90.0° for the (6,0) complex. This also elongates the O2–H9 and O3–H10 bonds to 0.981 Å whereas the non-hydrogen bonding O2–H8 and O3–H11 bond distances are 0.965 Å, slightly below the O–H distances for the remaining O–H bonds, which are comparable to the 0.967 Å seen for the (6,0) complex.

For the most part, the four inner shell water molecules not participating in hydrogen-bonding interactions with the outer shell water molecule retain most of the structural integrity of the (6,0) ground state inner shell, i.e., the hydrogen atoms point towards adjacent oxygen atoms. However, the water molecules perpendicular to the outer shell water molecule bend away from the hydrogen bonding interaction with an O6–Ca–O7 angle of

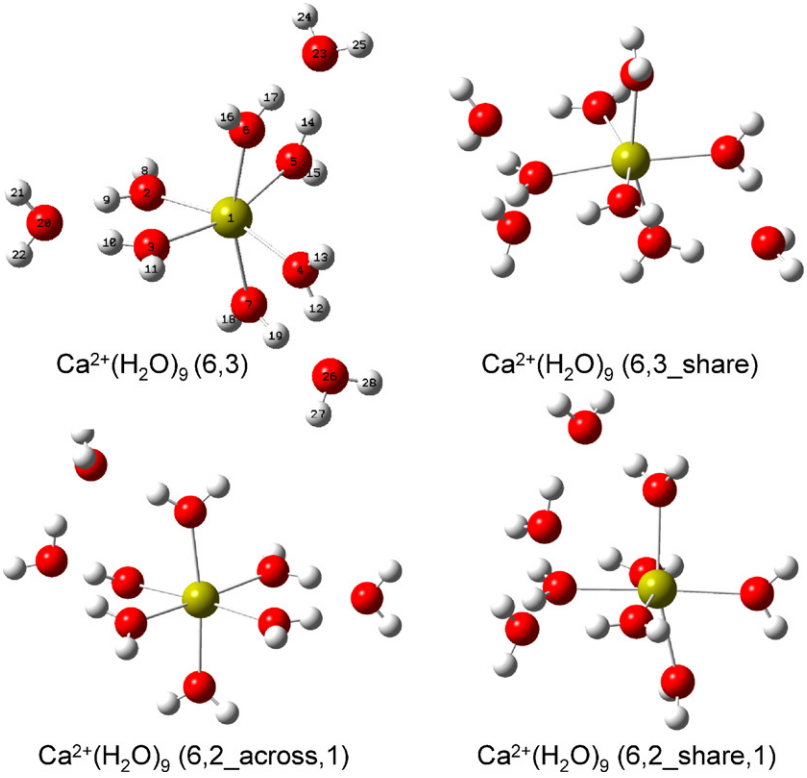

Fig. 8. Ground-state and low-lying geometries of $Ca^{2+}(H_2O)_9$. All structures were optimized at the B3LYP/6-311+G(d,p) level of theory.

163.3° and more towards O5 (O5–Ca–O6 and O5–Ca–O7 equal 83.3°) than to O4 (O4–Ca–O6 and O4–Ca–O7 equal 88.4°) because of the inner shell hydrogen bonds. The H–O–H angles for the hydrogen-bonding inner shell water molecules increase from 105.4° for (6,0) to 107.0° (O2) and 106.4° (O3) in (6,1). The former has a larger water angle because its non-hydrogen bonding hydrogen atom (H8) points directly towards an adjacent oxygen atom (O5), whereas the latter water molecule's

Table 3
B3LYP/6-311+G(d,p) geometry optimized structures for ground state $Ca^{2+}(H_2O)_{7–9}$

Complex	Symmetry	r(CaO) (Å)[a]	∠OCaO (°)[b]	∠CaOH (°)[c]	r(OH) (Å)[c,d]	r(O···H) (Å)[e]	∠HOH (°)
$Ca^{2+}(H_2O)_7$	C_1	2.405	79.7, 83.4 (2), 88.3 (2), 89.1, 92.2 (2), 95.3, 95.9, 96.8 (2), 166.3, 175.0, 175.6	127.0 (2)	0.967 (8)		105.8
		2.416 (2)		126.6/127.2 (2)			105.4 (2)
		2.422		130.6/124.2			105.2
		2.380 (2)		121.4/131.7	0.981/0.965 (2)	1.860 (2)	107.0
				119.8/133.8			106.4
		4.175		127.4 (2)	0.968 (2)		105.2
$Ca^{2+}(H_2O)_8$	C_2	2.421 (2)	77.6 (2), 84.7, 87.1 (2), 87.7 (2), 93.7 (2), 102.8 (2), 105.5, 161.2 (2), 165.8	124.3/130.2 (2)	0.966 (4)		105.6 (2)
		2.386 (4)		122.7/129.7 (2)	0.979/0.965 (4)	1.869 (4)	107.0 (4)
				122.8/130.3 (2)			
		4.233 (2)		126.4/128.3 (2)	0.968 (4)		105.3 (2)
$Ca^{2+}(H_2O)_9$	D_3	2.392 (6)	78.2 (3), 90.9 (6), 102.3 (3), 162.5 (3)	122.4/130.0 (6)	0.978/0.964 (6)	1.880 (6)	107.1 (6)
		4.234 (3)		127.3 (6)	0.967 (6)		105.3 (3)

Numbers in parentheses denote degeneracies.

[a] CaO distances for inner shell water molecules hydrogen unbound to outer shell molecules are listed first, followed by the inner shell molecules bound to outer shell water molecules, followed by outer shell molecules.

[b] Inner shell water molecules only.

[c] The first of two numbers separated by "/" denotes the angle or bond distance for a hydrogen atom participating in a hydrogen bond or one that points towards a hydrogen bonding interaction. The second number refers to the non-hydrogen bonding hydrogen atom.

[d] Covalent hydrogen-oxygen bond distances.

[e] Hydrogen bond distance between an inner shell hydrogen atom and outer shell oxygen atom.

non-hydrogen bonding hydrogen atom (H11) points towards a neighboring water molecule's hydrogen atom (H12). These interactions, a result of the rotation of the O3 water molecule to accommodate binding of the outer shell ligand, are sufficient to explain a number of distortions observed in the (6,1) structure. For example, the different environments of the O2 and O3 water molecules lead to Ca–O–H angles of 121.4° (Ca–O2–H9) and 119.8° (Ca–O3–H10), whereas their non-hydrogen bonding hydrogen atoms have angles of 131.7° (Ca–O2–H8) and 133.8° (Ca–O3–H11). Evidence for continued inner shell hydrogen bonding interactions come from observing that the O5 water molecule, which has interactions with both O6 and O7, has the largest H–O–H angle (105.8°). The O6 and O7 water molecules have 105.4° H–O–H angles, nearly identical with the (6,0) complex. The outer shell water molecule in the $Ca^{2+}(H_2O)_7$ complex has an angle (105.2°) very similar to that of a free water molecule (105.1°).

For the (6,2) and (6,3) complexes, the Ca–O bond distances for inner shell water molecules that hydrogen bond to outer shell molecules are 2.386 (O2, O3, O5, and O6) and 2.392 (O2–O7) Å, respectively, an increase of 0.006 Å for each additional water molecule. The two inner shell water molecules (O4 and O7) not participating in hydrogen bonding interactions for the (6,2) complex have Ca–O bond distances of 2.421 Å, somewhat larger than the average of such water molecules in (6,1). The O–H bond distances for the outer shell water molecules and inner shell water molecules not participating in bonding outer shell water molecules are comparable at 0.966–0.968 Å for (6,1), (6,2), and (6,3). The outer shell Ca–O distances are almost identical for the (6,2) and (6,3) complexes (4.233 and 4.234 Å) and significantly larger than that for the (6,1) complex (4.175 Å). The hydrogen bond distances between outer shell water molecules and the inner shell hydrogen atoms increase by 0.009 and 0.011 Å going from the (6,1) to the (6,2) complex and from the (6,2) to the (6,3) complex, respectively.

The O–Ca–O bond angles between inner shell water molecules that hydrogen bond to the outer shell are 77.6° for the (6,2) complex and 78.2° for the (6,3) complex, compared with 79.7° for (6,1). In (6,2), the remaining pair of inner shell water molecules has an O4–Ca–O7 angle of 84.7°. The O–H bond distances of inner shell water molecules hydrogen bonding to outer shell water molecules decrease from 0.981 Å for (6,1) to 0.979 and 0.978 Å for the (6,2) and (6,3) structures, respectively. The O–H distances for the non-hydrogen bonding hydrogen atoms on these water molecules remain at 0.964–0.965 Å. All other O–H bond lengths remain at about 0.966–0.967 Å.

Some semblance of the inner shell hydrogen bonding that controls the detailed structure of the (6,0) complex remains in the (6,2) structure. H11 has an interaction with O4 and H15 with O7, as indicated by O3–Ca–O4 and O5–Ca–O7 bond angles of 87.7°. However, because of the water rotations needed for binding the outer shell water molecules, neither the O4 or O7 water molecules are still aligned with the adjacent Ca–O bonds. Rather they have rotated such that the H13–O4–Ca–O6 and H18–O7–Ca–O2 dihedral angles are −16.5°.

The outer shell water molecules have H–O–H angles of 105.3° for the (6,2) complex, comparable to the outer shell water molecule in the (6,1) complex. Unlike the symmetric 127.4° Ca–O20–H21 and Ca–O20–H22 angles of the (6,1) complex, asymmetric 126.4° Ca–O20–H21 (Ca–O23–H24) and 128.3° Ca–O20–H22 (Ca–O23–H25) angles exist for the (6,2) complex. H21 and H24 have H21–O20–Ca–O6 and H24–O23–Ca–O2 dihedral angles of 9.7° whereas H22 and H25 form H22–O20–Ca–O7 and H25–O23–Ca–O4 dihedral angles of 13.4° (where the second oxygen atom is chosen as the inner shell water molecule perpendicular to the outer shell water molecule). Not only is the degree to which the hydrogen atom is removed from the O–Ca–O plane important in describing the asymmetric behavior of the Ca–O–H angles for the outer shell water molecules, but also the proximity of hydrogen atoms H21 (H24) to H16 (H8) and H22 (H25) to H18 (H13) as described by the appropriate dihedral angles. H21–O20–O6–H16 and H24–O23–O2–H8 dihedral angles are 39.2° and H22–O20–O7–H18 and H25–O23–O4–H13 dihedral angles are 28.8°. The larger dihedral angles occur because H21 (H24) sees a more exposed O6 (O2) oxygen atom and thus is in a more attractive environment. The smaller dihedral angles occur because H22 (H25) interacts not with O7 (O4), but instead with H18 (H13), yielding a long-range repulsive environment.

The inner shell water molecules of the (6,3) complex are all in the same environment with 107.1° H–O–H angles. There may be some residual of the inner shell hydrogen bonding interactions evident in the (6,0) complex as evidenced by the fact that all hydrogen atoms of the inner shell water molecules not involved in hydrogen bonding with outer shell water molecules point towards the adjacent oxygen atoms of neighboring water molecules. This weak interaction results in having these hydrogen atoms removed from the O–Ca–O plane by 4.0°, as described by the appropriate H–O–Ca–O dihedral angles. The Ca–O–H angles for these six specific hydrogen atoms are 130.0°, compared with 122.4° for the remaining inner shell water molecules.

The three outer shell water molecules have 105.3° H–O–H angles which are identical to the water molecules for the (6,2) complex, and comparable to the 105.2° H–O–H angle of the (6,1) complex. Unlike the (6,2) complex, the hydrogen atoms of the outer shell water molecules form identical 127.3° Ca–O–H angles because all the hydrogen atoms are removed from the O–Ca–O plane by 9.6° as defined by the H21–O20–Ca–O6 and H22–O20–Ca–O7 dihedral angles (O23 and O26 hydrogen atoms as well).

3.9. Conversion from 0 to 298 K

$\Delta H_{298} - \Delta H_0$ and $T\Delta S_{298}$ values, Table 4, are calculated with a rigid rotor/harmonic oscillator approximation using the vibrational frequencies and rotational constants calculated at the B3LYP/6-311+G(d,p) level of theory. The uncertainties for these values are found by scaling the vibrational frequencies up and down by 10%. These conversion factors are used to determine the ΔH_{298} and ΔG_{298} values listed in Table 4.

The $T\Delta S_{298}$ values increase going from $Ca^{2+}(H_2O)_5$ to $Ca^{2+}(H_2O)_6$, decrease for $Ca^{2+}(H_2O)_7$, and increase once again for the larger $Ca^{2+}(H_2O)_8$ and $Ca^{2+}(H_2O)_9$ complexes. This

Table 4
Conversion between 0 K enthalpies for H_2O loss from ground state $Ca^{2+}(H_2O)_x$ ($x = 5$–9) to enthalpies and free energies at 298 K in kJ/mol

Complex	ΔH_0[a]	$\Delta H_{298} - \Delta H_0$[b]	ΔH_{298}	$T\Delta S_{298}$[b]	ΔG_{298}
$Ca^{2+}(H_2O)_5$	112.8 (5.8)	2.2 (0.5)	115.0 (5.8)	40.5 (1.3)	70.7 (5.9)
$Ca^{2+}(H_2O)_6$	88.9 (5.0)	1.8 (0.5)	90.7 (5.0)	47.1 (1.4)	43.6 (5.2)
$Ca^{2+}(H_2O)_7$	60.0 (6.0)	3.7 (0.4)	63.7 (6.0)	33.0 (1.0)	30.7 (6.1)
$Ca^{2+}(H_2O)_8$	58.9 (3.2)	4.4 (0.5)	63.3 (3.2)	46.4 (1.0)	16.9 (3.4)
$Ca^{2+}(H_2O)_9$	57.8 (2.8)	4.3 (0.5)	62.1 (2.8)	47.2 (1.0)	15.2 (3.0)

Uncertainties are in parentheses.
[a] Experimental values from this work (Table 1).
[b] Values were calculated using standard formulae and molecular constants calculated at the B3LYP/6-311+G(d,p) level. Uncertainties correspond to scaling the vibrational frequencies up and down by 10%.

is a clear indication of the formation of a second solvent shell. Like the hydration enthalpies, ΔH_{298}, the free energies of hydration, ΔG_{298}, decrease as the size of the $Ca^{2+}(H_2O)_x$ complex increases. The $\Delta\Delta G_{298}$ (difference between ΔG_{298} of $Ca^{2+}(H_2O)_x$ and $Ca^{2+}(H_2O)_{x-1}$) values decrease monotonically from $Ca^{2+}(H_2O)_5$ to $Ca^{2+}(H_2O)_9$, but the free energies do not exhibit the same large decrease between $Ca^{2+}(H_2O)_6$ and $Ca^{2+}(H_2O)_7$ as the enthalpy values. This change occurs because of the large entropy change between the $Ca^{2+}(H_2O)_6$ and $Ca^{2+}(H_2O)_7$ complexes.

We also calculated the ΔG_{298} values for all additional structures of $x = 5$–9 shown in Figs. 4–8. For $x = 5$ and 6, the calculated ΔG_{298} excitation energies for the (4,1) and (4,2) structures increase compared to the ΔH_{298} values given in the text above by 3.1 and 5.4 kJ/mol. For $x = 6$, the calculated ΔG_{298} excitation energies for the (5,1_single) and (5,1_bridge) complexes decrease with respect to ΔH_{298} values by 13.1 and 9.6 kJ/mol. These changes still put the ΔG_{298} for the (5,1_bridge) complex 3.7, 0.4, and 13.4 kJ/mol higher than the (6,0) complex. For the second solvent shell structures of $x = 7$–9, the calculated ΔG_{298} excitation energies decrease with respect to the ΔH_{298} values (positive $T\Delta S_{298}$ terms), with two exceptions: the (5,2) and (6,2_across) structures. Most notably, the second lowest energy structures for $x = 8$ and 9, (6,2_share) and (6,3_share) now have ΔG_{298} excitation energies of 1.5, 2.0 and 1.9 and −2.6, −2.4, and −2.8 kJ/mol, making them comparable in energy to the (6,2) and (6,3) structures. Because the relative free energies of these structures are comparable, it is likely that the ESI source produces a distribution of these structures; however, because the energetics are virtually identical, this will not affect the data analysis or the final bond enthalpies measured. We verified that data analysis using molecular parameters for the alternate structures did not change the parameters of Eq. (2) listed in Table 1.

3.10. Theoretical bond enthalpies

Theoretical bond enthalpies for losing a single water molecule from all $Ca^{2+}(H_2O)_x$ complexes are listed in Table 5. These enthalpies include ZPE and thermal corrections to 298 K both with and without BSSE corrections and are calculated

Table 5
Theoretical 298 K bond enthalpies for H_2O loss from ground state $Ca^{2+}(H_2O)_x$ ($x = 1$–9) in kJ/mol

Geometry[a]	Single point[b]	$x = 1$	2	3	4	5	6	7	8	9	MAD[c]
MP2(full)[d]	B3LYP	228 (229)	197 (199)	172 (174)	148 (149)	114 (115)	102 (104)	74 (77)	77 (80)	73 (76)	1 ± 1 (1 ± 1)
B3LYP/	B3LYP	229 (230)	197 (199)	172 (174)	147 (149)	113 (116)	101 (104)	74 (77)	77 (80)	73 (76)	
6-311+G(d,p)	B3P86	228 (230)	196 (198)	171 (173)	146 (148)	114 (116)	101 (104)	77 (80)	79 (82)	75 (78)	1 ± 1 (1 ± 1)
	MP2(full)	212 (216)	188 (194)	168 (174)	147 (152)	120 (127)	108 (117)	73 (82)	76 (85)	72 (81)	5 ± 5 (7 ± 5)
B3LYP/	B3LYP	234 (234)	200 (200)	173 (173)	147 (148)	113 (113)	101 (102)	74 (75)	77 (78)	73 (74)	1 ± 2 (2 ± 1)
aug-cc-pVTZ	B3P86	234 (235)	199 (200)	172 (173)	147 (147)	113 (113)	101 (102)	77 (78)	78 (80)	75 (76)	2 ± 2 (2 ± 2)
(Ca-G)	MP2(full)	220 (224)	193 (198)	171 (175)	149 (155)	120 (126)	109 (117)	77 (86)	79 (88)	75 (84)	4 ± 3 (7 ± 4)
	MP2(FC)	219 (222)	193 (196)	171 (173)	149 (152)	120 (124)	109 (113)	77 (82)	80 (84)	76 (80)	4 ± 3 (5 ± 3)
Pavlov et al.[e]		(236)	(200)	(177)	(151)	(118)	(105)	(77)	(39)		(2 ± 2)
GF[f]		224	198	179	157	126	114				8 ± 5
Merrill et al.[g]		(220)	(196)	(177)	(157)	(129)	(117)				(10 ± 6)
Katz et al.[h]		(235)	(216)	(200)	(179)	(143)	(133)	(90)	(85)	(57)	(22 ± 10)

Values in parentheses do not include BSSE corrections.
[a] Theory level used for geometry optimization.
[b] Theory level used for single point energy calculations using either 6-311+G(2d,2p) or aug-cc-pVTZ basis sets (see text).
[c] Mean absolute deviation from the B3LYP/6-311+G(2d,2p)//B3LYP/6-311+G(d,p) results. Uncertainties are one standard deviation of the absolute deviations.
[d] Basis set was 6-311+G(d,p).
[e] [17].
[f] Glendening and Feller [18].
[g] [19].
[h] [20].

for the lowest energy structures, shown in Figs. 3–8. Single point energies at the B3LYP, B3P86, and MP2(full) levels using a 6-311+G(2d,2p) basis set were calculated from geometry optimizations using B3LYP and MP2(full) with a 6-311+G(d,p) basis set. Results for the MP2(full) geometries are shown in Table 5 only for the B3LYP bond energies because the two geometries produce nearly identical bond enthalpies for $x = 1$–9 (differences less than 1 kJ/mol). The B3LYP and B3P86 single point calculations produce almost identical binding enthalpies for $Ca^{2+}(H_2O)_x$, where $x = 1$–6, but B3LYP values are 2–3 kJ/mol lower than B3P86 binding enthalpies for $x = 7$–9. MP2(full) provides lower binding enthalpies for $x = 1$–3, higher values for $x = 5$ and 6, and slightly lower values for $x = 7$–9 compared with B3LYP single point enthalpies. The BSSE corrections are 1–3 kJ/mol for DFT bond energies with either B3LYP or MP2(full) geometry optimizations, but much larger, 4–9 kJ/mol, for MP2(full) bond energies.

Compared to results obtained using the 6-311+G(2d,2p) basis set, bond energies using the aug-cc-pVTZ(Ca-G) basis set yielded smaller BSSE corrections, less than 1.0 kJ/mol for DFT bond energies. BSSE corrections at the MP2(full)/aug-cc-pVTZ(Ca-G) and MP2(FC)/aug-cc-pVTZ(Ca-G) levels of theory are larger, 4–9 and 2–5 kJ/mol, respectively. Nevertheless, binding enthalpies calculated at the B3LYP and B3P86 levels with the aug-cc-pVTZ(Ca-G) basis set produce very similar results to values calculated using the 6-311+G(2d,2p) basis set. Values for $x = 3$–9 are essentially identical and values for the smallest complexes are slightly larger (3–6 kJ/mol) for the aug-cc-pVTZ(Ca-G) basis set. Somewhat larger differences occur for the MP2(full)/aug-cc-pVTZ(Ca-G)//B3LYP/aug-cc-pVTZ(Ca-G) calculations compared with the MP2(full)/6-311+G(2d,2p)//B3LYP/6-311+G(d,p) calculations.

At the suggestion of a reviewer, we also performed calculations using correlation consistent basis sets for calcium, specifically cc-pVTZ, cc-pCVTZ, and cc-pwCVTZ along with the aug-cc-pVTZ basis set on water, for $x = 1$–6 (not provided in Table 5). Regardless of the correlation consistent basis set chosen for calcium, the B3LYP and B3P86 bond energies are essentially identical to one another and to the aug-cc-pVTZ(Ca-G) results, all lying within 2 kJ/mol of one another. Larger variations are observed for the MP2 results although no differences in the MP2(full) versus MP2(FC) bond energies were observed. Here the aug-cc-pVTZ(Ca-G) and aug-cc-pVTZ results are essentially identical, whereas the aug-cc-pVTZ(Ca-C) and aug-ccpVTZ(Ca-wC) are higher by 1–5 kJ/mol, with a MAD compared to aug-cc-pVTZ(Ca-G) of 2 ± 1 kJ/mol. Overall, the bond energies obtained using the aug-cc-pVTZ(Ca-G) basis set, Table 5, is representative of this entire class of calculations.

It is useful to provide one additional observation regarding the calculations using frozen core MP2, MP2(FC), performed using all variations of the aug-cc-pVTZ basis set. For MP2(FC) calculations of Ca^{2+}, the Gaussian03 default uses a small 10-electron core corresponding to the 1s, 2s, and 2p electrons, but switches to an 18-electron core when calcium complexes to any number of water molecules. To avoid this change in the default conditions, the MP2(FreezeG2) command, which freezes the 10-electron core of Ca^{2+} and the 1s electrons of the oxygen atoms, is used.

The deviations among the various theoretical methods listed in Table 5 can be compared succinctly using the calculated mean absolute deviation (MAD) with respect to the B3LYP(6-311+G(2d,2p))//B3LYP binding energies. Very small differences are found between the results obtained using the 6-311+G(2d,2p) and aug-cc-pVTZ(Ca-G) basis sets and between B3LYP and B3P86 single point energies. Somewhat larger deviations are found for the MP2 methods, with lack of BSSE corrections yielding the biggest differences. Given these comparisons, the B3LYP/6-311+G(2d,2p)//B3LYP/6-311+G(d,p) (B3LYP//B3LYP) binding energies are representative of our calculated theoretical results at all levels.

3.11. Literature calculations

Table 5 also lists results from a number of theoretical studies in the literature, which employ a diverse group of basis sets and levels of theory in determining their binding enthalpies. All of these studies treat the calcium ion basis set in some special way compared to the light atoms. Katz et al. [20] performed single point energy calculations for $Ca^{2+}(H_2O)_x$, $x = 1$–9, where all water molecules were bound directly to the calcium ion using a MP2(full)/HUZSP*(p,d)//RHF/HUZSP*(p) level with ZPE and thermal corrections taken from the RHF/HUZSP*(p) frequency calculations. This basis set comprises a standard 6-31G(d) basis set for the light atoms and a split valence Huzinaga basis set for the calcium ion, where no diffuse functions are included. This study also computed relative energies for the $Ca^{2+}(H_2O)_x$ complexes where $x = 6$–8 with varying number of water molecules bound directly to the calcium ion, and these calculations included diffuse functions on all of the atoms. Glendening and Feller [18] calculated hydration energies for $Ca^{2+}(H_2O)_x$, $x = 1$–6, employing a MP2(FC)/6-31+G(d)//RHF/6-31+G(d) level of theory. For the geometry optimization and single point energy calculations, Hay/Wadt ECP treatment of the calcium atom (10-core electrons) was used and correlation of the 1s electrons on oxygen was neglected. ZPE, thermal, and BSSE corrections were included in this study.

Merrill et al. [19] have utilized an effective fragment potential approach for $Ca^{2+}(H_2O)_x$, $x = 1$–6 where only the metal cation is treated with an ab initio wavefunction. This approach is used to reproduce Hartree-Fock binding energies with the 6-31+G(d) basis set. The energies include ZPE and thermal corrections, but no BSSE correction because the water molecules have no basis functions. Pavlov et al. [17] have studied $Ca^{2+}(H_2O)_x$ complexes where $x = 1$–8 with density functional theory (B3LYP) that includes a Hay/Wadt ECP treatment for calcium and a LANL2DZ basis set for the smaller atoms in the geometry optimization. The $Ca^{2+}(H_2O)_7$ complex has six water molecules in the inner hydration shell with the outer shell water molecule participating in two hydrogen bonds, (6,1). The binding energy for the $Ca^{2+}(H_2O)_8$ complex is calculated with all eight water molecules in the first solvent shell, (8,0). B3LYP/6-311+G(2d,2p) was used for subsequent single point

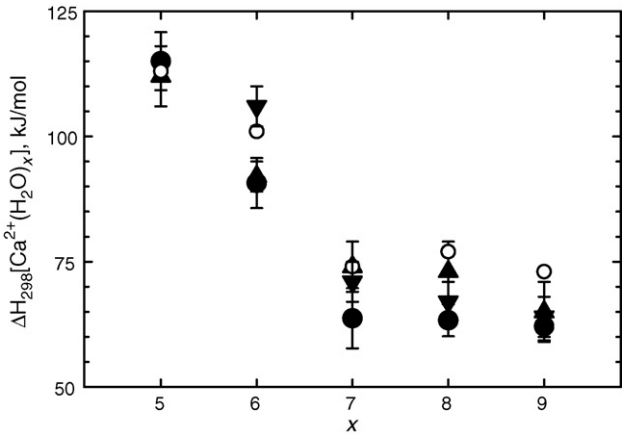

Fig. 9. Comparison of experimental (solid symbols) and theoretical (open symbols, B3LYP//B3LYP) bond enthalpies at 298 K. Present results are shown by circles. HPMS results from Ref. [10] are down triangles and BIRD results from Refs. [15] and [16] are triangles.

energy calculations that include ZPE corrections. In this case, the values listed in Table 5 have been adjusted to 298 K using thermal corrections taken from our calculations. This procedure for optimizing $Ca^{2+}(H_2O)_x$ structures and calculating their single point energies closely resembles our theoretical approach.

4. Discussion

4.1. Comparison between present and literature experimental values

Kebarle and coworkers [10,14] and Williams and coworkers [15,16] have previously reported hydration enthalpies at 298 K for the $Ca^{2+}(H_2O)_x$ systems where $x = 6$–14 and 5–10, respectively. Fig. 9 shows that our experimental results agree within experimental uncertainty with these previous experimental results and that the same qualitative trends are observed. A more quantitative comparison shows that our experimental numbers agree best with those of the BIRD experiments of Williams and coworkers for the inner shell complexes, $Ca^{2+}(H_2O)_5$ and $Ca^{2+}(H_2O)_6$ complex (Table 6). For the larger complexes, $Ca^{2+}(H_2O)_7$ and $Ca^{2+}(H_2O)_8$, our experimental results agree within the combined experimental uncertainties with the HPMS results of Kebarle and coworkers, whereas the BIRD results, which are slightly higher, are at the edge of the combined experimental uncertainties. For $Ca^{2+}(H_2O)_9$, all three experimental bond enthalpies agree well. It is possible that our experimental numbers for the $Ca^{2+}(H_2O)_7$, $Ca^{2+}(H_2O)_8$, and $Ca^{2+}(H_2O)_9$ complexes are slightly low because the ions are not completely thermalized, which would shift the thresholds for CID to lower energies. For instance, it may be the ions have reached equilibrium at the capillary temperature used for these larger systems, 80 °C, although recent experiments suggest that thermalization of the ions occurs primarily in the hexapole ion trap, which is at room temperature [24]. If the data are analyzed using 80 °C as the reactant temperature, our binding enthalpies increase by 4 kJ/mol for the $Ca^{2+}(H_2O)_7$, $Ca^{2+}(H_2O)_8$, and $Ca^{2+}(H_2O)_9$ complexes. Ideally, such a temperature increase could be evaluated by examining these CID processes at multiple capillary temperatures, however, the range of capillary temperatures providing stable and sufficiently intense ion beams is limited.

Table 6
Experimental and theoretical 298 K bond enthalpies for H_2O loss from ground state $Ca^{2+}(H_2O)_x$ ($x = 1$–9) in kJ/mol

Complex	This work	HPMS[a]	BIRD[b]	Theory[c]
$Ca^{2+}(H_2O)$				229
$Ca^{2+}(H_2O)_2$				197
$Ca^{2+}(H_2O)_3$				172
$Ca^{2+}(H_2O)_4$				147
$Ca^{2+}(H_2O)_5$	115 (6)		112 (6)	113
$Ca^{2+}(H_2O)_6$	91 (5)	106 (4)	92 (3)	101
$Ca^{2+}(H_2O)_7$	64 (6)	71 (4)	74 (5)	74
$Ca^{2+}(H_2O)_8$	63 (3)	67 (4)	73 (6)	77
$Ca^{2+}(H_2O)_9$	62 (3)	64 (4)	65 (6)	73
MAD[d]	9 (4)	7 (3)	4 (4)	

Uncertainties are in parentheses.
[a] Values taken from Ref. [10]. Uncertainties were assigned in Ref. [16].
[b] Values taken from Refs. [15] and [16].
[c] B3LYP/6-311+G(2d,2p)//B3LYP/6-311+G(d,p) values from Table 5 including BSSE corrections.
[d] Mean absolute deviation from theoretical results.

4.2. Comparison between theory and experiment

Table 6 also compares the experimental 298 K bond enthalpies with B3LYP//B3LYP values computed here, which are representative of the many theoretical calculations performed here (Table 5). Our experimental values agree best with the B3LYP//B3LYP hydration enthalpies when BSSE corrections are included, as evidenced by a MAD decrease from 12 ± 6 kJ/mol without BSSE corrections to 9 ± 4 kJ/mol. Likewise, BSSE corrections always improved the agreement between experiment and theory for other levels of theory considered here. MADs for other levels of theory with BSSE corrections were comparable or slightly larger than for the B3LYP//B3LYP values: 11 ± 6 kJ/mol for B3P86//B3LYP, 11 ± 4 kJ/mol for MP2(full)//B3LYP, and 9 ± 5 kJ/mol for B3LYP//MP2(full). When the aug-cc-pVTZ(Ca-G) basis sets are used, the MADs versus experiment remain unchanged compared to the 6-311+G(d,p) analogues, except that the MADs for the MP2(full)//B3LYP and MP2(FC)//B3LYP results increase to 13 ± 5 kJ/mol.

The hydration enthalpies calculated from B3LYP/6-311+G(d,p) geometries show similar qualitative trends as the experimental results (Fig. 9). The enthalpies decrease monotonically from the $Ca^{2+}(H_2O)_5$ to the $Ca^{2+}(H_2O)_7$ complex. Binding enthalpies for the seventh, eighth, and ninth water molecules, which reside in the outer solvent shell that hydrogen bond to the inner shell water molecules, differ from one another by less than 5 kJ/mol at all levels of theory. Hydration enthalpies calculated from theory are 2–4 kJ/mol higher for the $Ca^{2+}(H_2O)_8$ complex compared with the $Ca^{2+}(H_2O)_7$ complex. The $Ca^{2+}(H_2O)_9$ complex is then 3–5 kJ/mol lower in energy than the $Ca^{2+}(H_2O)_8$ complex. Thus, the $Ca^{2+}(H_2O)_7$ and $Ca^{2+}(H_2O)_9$ complexes have theoretical hydration enthalpies

that are within 1–2 kJ/mol of one another. These theoretical trends in the $x = 7$–9 bond enthalpies agree somewhat better with our results, where the values change little, compared to the HPMS and BIRD results where the bond enthalpies decrease systematically by 7–9 kJ/mol from $Ca^{2+}(H_2O)_7$ to $Ca^{2+}(H_2O)_9$.

From a quantitative standpoint, our experimental values for the $x = 5$–9 complexes are consistently lower than B3LYP//B3LYP theoretical calculations. Experimental values for $x = 5$ and 6 are within 9 kJ/mol of the theory values. Experimental second shell complexes have hydration enthalpies 11–14 kJ/mol lower than the calculations. Because the HPMS and BIRD values are slightly larger than our experimental values, the agreement with theory is better. Compared to the B3LYP//B3LYP results, the MADs for the literature results are 7 ± 3 and 4 ± 4 kJ/mol, respectively.

4.3. Comparison with theoretical results from the literature

A host of theoretical studies of the $Ca^{2+}(H_2O)_x$ system, where $x = 1$–7, can be found in the literature. The results from four studies are shown along with our theoretical calculations in Table 5. The hydration enthalpies calculated by Pavlov et al. [17] do not include BSSE corrections, and therefore resemble our B3LYP/6-311+G(2d,2p)//B3LYP/6-311+G(d,p) single point energies without BSSE corrections as evidenced by a MAD of 2 ± 2 kJ/mol, Table 5, although these results are systematically higher than the B3LYP//B3LYP values. This MAD excludes the value for the $Ca^{2+}(H_2O)_8$ complex because the literature value refers to a geometry where all water ligands were bound directly to the calcium ion. As noted above, we find this structure to lie 42 kJ/mol higher in energy at the B3LYP//B3LYP level, accounting for the quantitative difference in the two calculated bond enthalpies.

BSSE corrected single point energies calculated by Glendening and Feller [18] have a MAD of 8 ± 5 kJ/mol with respect to our B3LYP//B3LYP energies and are systematically higher. It seems likely that the bond energies of Glendening and Feller would decrease if a more advanced level of theory that accounts for electron correlation was used for the geometry optimization and larger basis sets with additional polarization functions were used for subsequent single point energies. Single point energy calculations determined by Merrill et al. [19] using the effective fragment potential produces comparable single point energies with those from Glendening and Feller [18] with a MAD of 10 ± 6 kJ/mol with respect to our B3LYP/B3LYP energies. Finally, the theoretical results taken from Katz et al. [20] are much higher than all other theoretical approaches (MAD of 22 ± 10 kJ/mol compared to B3LYP//B3LYP). These calculations do not incorporate diffuse functions into their basis sets for geometry optimizations or single point energy calculations, which result in significantly larger binding energies.

Katz et al. [20] also calculated the relative binding energies for $x = 6$–8 to determine the number of water molecules that prefer to bind directly to the calcium ion. Even with their single point energy basis set now augmented by diffuse functions, their calculated relative MP2(full) energies for the $Ca^{2+}(H_2O)_6$ (5,1) and (4,2) structures lie 34 and 63 kJ/mol higher in energy than the ground state (6,0) structure, which is roughly 1.3–1.5 times larger than our MP2(full)/6-311+G(2d,2p)//B3LYP/6-311+G(d,p) single point energies of 23 and 47 kJ/mol. In agreement with the present results, Katz et al. determined that six water molecules prefer to bind directly to the calcium ion with additional water molecules hydrogen bonding to inner shell water molecules for the $Ca^{2+}(H_2O)_7$ and $Ca^{2+}(H_2O)_8$ complexes. Katz et al. find relative energies for the (7,0) and (8,0) structures, where all water molecules are bound directly to the calcium ion, with respect to the (6,1) and (6,2) ground states for $Ca^{2+}(H_2O)_7$ and $Ca^{2+}(H_2O)_8$, were 6 and 2 kJ/mol, respectively. Our MP2//B3LYP results suggest that overcrowding the inner shell leads to single point energies of 10 and 17 kJ/mol higher than the (6,1) and (6,2) ground states, respectively, and the DFT calculations find these structures are even higher (about 22 and 42 kJ/mol, respectively). The overestimation of the relative single point energies for the $Ca^{2+}(H_2O)_6$ structure and underestimation of the $Ca^{2+}(H_2O)_7$ and $Ca^{2+}(H_2O)_8$ structures results from the restricted Hartree-Fock treatment for the geometry optimizations used by Katz et al.

5. Conclusion

The kinetic energy dependent cross sections for $Ca^{2+}(H_2O)_x$ complexes where $x = 5$–9 are determined by collision-induced dissociation using a guided ion beam tandem mass spectrometer with a new electrospray ionization source [24]. The results reported here represent our first comprehensive study of multiply charged ions with this new source. The dominant process taking place in all systems studied here is the loss of a single water molecule from the parent species. An additional proton transfer/charge separation process is also observed once the $Ca^{2+}(H_2O)_2$ complex forms from sequential dissociation of the larger complexes. At this point, the $Ca^{2+}(H_2O)_2$ complex can lose one of its water molecules or form two singly charged particles, $CaOH^+$ and H_3O^+. Future experimental work will delve into these types of competitive processes and the CID of the smallest $Ca^{2+}(H_2O)_x$ complexes, $x = 1$–4, systems for which measurement of the bond energies is inaccessible to other experimental techniques.

Our experimental results for the $Ca^{2+}(H_2O)_x$ ($x = 5$–9) system agree well with other experimental techniques found in the literature [10,14–16]. Binding energies decrease monotonically from $Ca^{2+}(H_2O)_5$ to $Ca^{2+}(H_2O)_7$. The binding energies for the $Ca^{2+}(H_2O)_7$, $Ca^{2+}(H_2O)_8$, and $Ca^{2+}(H_2O)_9$ complexes differ by less than 2 kJ/mol, suggesting the binding motifs of these three water molecules are very similar. This suggests that six water molecules bind directly to the calcium ion, in agreement with theory. Binding energies obtained for these second shell complexes tend to be a bit lower than HPMS [10,14] and BIRD [15,16] studies, but still fall within experimental uncertainties.

Our theoretical calculations of the structures and energetics for the $Ca^{2+}(H_2O)_x$ ($x = 1$–9) system represent the first comprehensive study of the ion's hydration throughout this range. We find that six water molecules bind directly to the calcium ion in agreement with previous work [17–20]. For the $Ca^{2+}(H_2O)_x$ complexes ($x = 7$–9), the additional outer shell

water molecules hydrogen bond to pairs of the six inner shell water molecules using the same structural motif. Alternate structures for $Ca^{2+}(H_2O)_7$, $Ca^{2+}(H_2O)_8$, and $Ca^{2+}(H_2O)_9$ complexes have been qualitatively and quantitatively discussed in detail with respect to the lowest energy structures. The present results demonstrate that accurate calculations of the binding energies must include diffuse functions for the geometry optimization and subsequent single point energy calculations and also take into account BSSE corrections. From our theoretical study of the $Ca^{2+}(H_2O)_x$ complexes where $x = 1$–9, it appears that B3LYP/6-311+G(d,p) geometry optimizations and subsequent B3LYP/6-311+G(2d,2p) single point energies provide reasonable agreement with experiment and should be sufficient for future hydration studies.

Acknowledgements

Funding for this work was provided by the National Science Foundation under Grant No. CHE-0451477. D.R.C. wishes to thank R.M. Moision for introducing him to electrospray ionization and the GIBMS and C.R. Iceman for useful discussions. Thanks to the reviewer for several useful comments regarding the calculations.

References

[1] H. Lodish, A. Berk, P. Matsudaira, C.A. Kaiser, M. Krieger, M.P. Scott, S.L. Zipursky, Molecular Cell Biology, W.H. Freeman and Company, New York, 2004.
[2] I. Dzidic, P. Kebarle, J. Phys. Chem. 74 (1970) 1466.
[3] S.K. Searles, P. Kebarle, Can. J. Chem. 47 (1969) 2619.
[4] P.M. Holland, A.W. Castleman Jr., J. Chem. Phys. 76 (1982) 4195.
[5] N.F. Dalleska, B.L. Tjelta, P.B. Armentrout, J. Phys. Chem. 98 (1994) 4191.
[6] N.F. Dalleska, K. Honma, L.S. Sunderlin, P.B. Armentrout, J. Am. Chem. Soc. 116 (1994) 3519.
[7] H. Koizumi, M. Larson, F. Muntean, P.B. Armentrout, Int. J. Mass Spectrom. 228 (2003) 221.
[8] M.T. Rodgers, P.B. Armentrout, J. Phys. Chem. A 101 (1997) 1238.
[9] S.G. Lias, in: P.J. Linstrom, W.G. Mallard (Eds.), "Ionization Energy Evaluation" NIST Chemistry WebBook, National Institute of Standards and Technology, Gaithersburg, MD, June 2005, p. 20899, http://webbook.nist.gov.
[10] M. Peschke, A.T. Blades, P. Kebarle, J. Phys. Chem. A 102 (1998) 9978.
[11] A.A. Shvartsburg, K.W.M. Siu, J. Am. Chem. Soc. 123 (2001) 10071.
[12] M. Yamashita, J.B. Fenn, J. Phys. Chem. 88 (1984) 4451.
[13] C.M. Whitehouse, R.N. Dreyer, M. Yamashita, J.B. Fenn, Anal. Chem. 57 (1985) 675.
[14] A.T. Blades, P. Jayaweera, M.G. Ikonomou, P. Kebarle, J. Chem. Phys. 92 (1990) 5900.
[15] S.E. Rodriguez-Cruz, R.A. Jockusch, E.R. Williams, J. Am. Chem. Soc. 121 (1999) 8898.
[16] R.L. Wong, K. Paech, E.R. Williams, Int. J. Mass Spectrom. 232 (2004) 59.
[17] M. Pavlov, P.E.M. Siegbahn, M. Sandstrom, J. Phys. Chem. A 102 (1998) 219.
[18] E.D. Glendening, D. Feller, J. Phys. Chem. 100 (1996) 4790.
[19] G.N. Merrill, S.P. Webb, D.B. Bivin, J. Phys. Chem. A 107 (2003) 386.
[20] A.K. Katz, J.P. Glusker, S.A. Beebe, C.W. Bock, J. Am. Chem. Soc. 118 (1996) 5752.
[21] K.M. Ervin, P.B. Armentrout, J. Chem. Phys. 83 (1985) 166.
[22] F. Muntean, P.B. Armentrout, J. Chem. Phys. 115 (2001) 1213.
[23] N. Aristov, P.B. Armentrout, J. Phys. Chem. 90 (1986) 5135.
[24] R.M. Moision, P.B. Armentrout, J. Am. Soc. Mass Spectrom., in press.
[25] S.A. Shaffer, D.C. Prior, G.A. Anderson, H.R. Udseth, R.D. Smith, Anal. Chem. 70 (1998) 4111.
[26] S.A. Shaffer, A. Tolmachev, D.C. Prior, G.A. Anderson, H.R. Udseth, R.D. Smith, Anal. Chem. 71 (1999) 2957.
[27] T. Kim, A.V. Tolmachev, R. Harkewicz, D.C. Prior, G. Anderson, H.R. Udseth, R.D. Smith, Anal. Chem. 72 (2000) 2247.
[28] D. Gerlich, Adv. Chem. Phys. 82 (1992) 1.
[29] S.E. Stein, B.S. Rabinovitch, Chem. Phys. Lett. 49 (1977) 1883.
[30] T.S. Beyer, D.F. Swinehart, Comm. Assoc. Comput. Mach. 16 (1973) 379.
[31] S.E. Stein, B.S. Rabinovich, J. Chem. Phys. 58 (1973) 2438.
[32] R.G. Gilbert, S.C. Smith, Theory of Unimolecular and Recombination Reactions, Blackwell Scientific, Oxford, 1990.
[33] D.A. Hales, L. Lian, P.B. Armentrout, Int. J. Mass Spectrom. Ion Process. 102 (1990) 269.
[34] R.H. Schultz, K.C. Crellin, P.B. Armentrout, J. Am. Chem. Soc. 113 (1991) 8590.
[35] S.K. Loh, D.A. Hales, L. Lian, P.B. Armentrout, J. Chem. Phys. 90 (1989) 5466.
[36] F.A. Khan, D.E. Clemmer, R.H. Schultz, P.B. Armentrout, J. Phys. Chem. 97 (1993) 7978.
[37] M.T. Rodgers, K.M. Ervin, P.B. Armentrout, J. Chem. Phys. 106 (1997) 4499.
[38] C. Iceman, P.B. Armentrout, Int. J. Mass Spectrom. 222 (2003) 329.
[39] M.T. Rodgers, P.B. Armentrout, JACS 122 (2000) 8548.
[40] J.C. Amicangelo, P.B. Armentrout, J. Phys. Chem. A 104 (2000) 11420.
[41] R.M. Moision, P.B. Armentrout, J. Phys. Chem. A 106 (2002) 10350.
[42] R.M. Moision, P.B. Armentrout, Phys. Chem. Chem. Phys. 6 (2004) 2588.
[43] R.M. Moision, P.B. Armentrout, J. Phys. Chem. A 110 (2006) 3933.
[44] D.G. Truhlar, B.C. Garrett, S.J. Klippenstein, J. Phys. Chem. 100 (1996) 12771.
[45] K.A. Holbrook, M.J. Pilling, S.H. Robertson, Unimolecular Reactions, Wiley, New York, 1996.
[46] P.B. Armentrout, J. Simons, J. Am. Chem. Soc. 114 (1992) 8627.
[47] E.V. Waage, B.S. Rabinovitch, Chem. Rev. 70 (1970) 377.
[48] M.J. Frisch, G.W. Trucks, H.B. Schlegel, G.E. Scuseria, M.A. Robb, J.R. Cheeseman, J.J.A. Montgomery, T. Vreven, K.N. Kudin, J.C. Burant, J.M. Millam, S.S. Iyengar, J. Tomasi, V. Barone, B. Mennucci, M. Cossi, G. Scalmani, N. Rega, G.A. Petersson, H. Nakatsuji, M. Hada, M. Ehara, K. Toyota, R. Fukuda, J. Hasegawa, M. Ishida, T. Nakajima, Y. Honda, O. Kitao, H. Nakai, M. Klene, X. Li, J.E. Knox, H.P. Hratchian, J.B. Cross, C. Adamo, J. Jaramillo, R. Gomperts, R.E. Stratmann, O. Yazyev, A.J. Austin, R. Cammi, C. Pomelli, J.W. Ochterski, P.Y. Ayala, K. Morokuma, G.A. Voth, P. Salvador, J.J. Dannenberg, V.G. Zakrzewski, S. Dapprich, A.D. Daniels, M.C. Strain, O. Farkas, D.K. Malick, A.D. Rabuck, K. Raghavachari, J.B. Foresman, J.V. Ortiz, Q. Cui, A.G. Baboul, S. Clifford, J. Cioslowski, B.B. Stefanov, G. Liu, A. Liashenko, P. Piskorz, I. Komaromi, R.L. Martin, D.J. Fox, T. Keith, M.A. Al-Laham, C.Y. Peng, A. Nanayakkara, M. Challacombe, P.M.W. Gill, B. Johnson, W. Chen, M.W. Wong, C. Gonzalez, J.A. Pople, Gaussian 03, Revision B.02, Gaussian, Inc., Pittsburgh, PA, 2003.
[49] A.D. Becke, J. Chem. Phys. 98 (1993) 5648.
[50] C. Lee, W. Yang, R.G. Parr, Phys. Rev. B 37 (1988) 785.
[51] C.W. Bauschlicher Jr., H. Partridge, J. Chem. Phys. 103 (1995) 1788.
[52] J.P. Perdew, Phys. Rev. B 33 (1986) 8822.
[53] C. Möller, M.S. Plesset, Phys. Rev. 46 (1934) 618.
[54] S.F. Boys, R. Bernardi, Mol. Phys. 19 (1970) 553.
[55] F.B. van Duijneveldt, J.G.C.M. van Duijneveldt de Rijdt, J.H. van Lenthe, Chem. Rev. 94 (1994) 1873.
[56] P.J. Hay, W.R. Wadt, J. Chem. Phys. 82 (1985) 299.
[57] D. Andrae, U. Haeussermann, M. Dolg, H. Stoll, H. Preuss, Theor. Chim. Acta 77 (1990) 123.
[58] D.E. Woon, T.H. Dunning, J. Chem. Phys. 98 (1993) 1358.
[59] J. Koput, K.A. Peterson, J. Phys. Chem. A 106 (2002) 9595.
[60] M.T. Rodgers, P.B. Armentrout, Int. J. Mass Spectrom., doi:10.1016/j.ijms.2007.02.034, in press.
[61] C.W. Bauschlicher, M. Sodupe, H. Partridge, J. Chem. Phys. 96 (1992) 4453.